2007-11-19

Microfluidic Electro-osmotic Flow Pumps

John Mason Edwards
Brigham Young University - Provo

MICROFLUIDIC ELECTRO-OSMOTIC FLOW PUMPS

by

John M. Edwards IV

A thesis submitted to the faculty of

Brigham Young University

in partial fulfillment of the requirements for the degree of

Master of Science

Department of Chemistry and Biochemistry

Brigham Young University

December 2007

BRIGHAM YOUNG UNIVERSITY

GRADUATE COMMITTEE APPROVAL

of a thesis submitted by

John M. Edwards IV

This dissertation has been read by each member of the following graduate committee and by majority vote has been found to be satisfactory.

_____	_____
Date	Milton L. Lee, Chair
_____	_____
Date	Aaron R. Hawkins
_____	_____
Date	Matthew R. Linford
_____	_____
Date	Adam T. Woolley

BRIGHAM YOUNG UNIVERSITY

As chair of the candidate's graduate committee, I have read the dissertation of John M. Edwards in its final form and have found that (1) its format, citation, and bibliographical style are consistent and acceptable and fulfill university and department style requirements; (2) its illustrated materials including figures, tables, and charts are in place; and (3) the final manuscript is satisfactory to the graduate committee and is ready for submission to the university library.

_____
Date

_____
Milton L. Lee
Chair, Graduate Committee

Accepted for the Department

_____
David V. Dearden
Graduate Coordinator

Accepted for the College

_____
Thomas W. Sederberg
Associate Dean, College of Physical
and Mathematical Sciences

ABSTRACT

MICROFLUIDIC ELECTRO-OSMOTIC FLOW PUMPS

John M. Edwards IV

Department of Chemistry and Biochemistry

Master of Science

The need for miniaturized, portable devices to separate and detect unknown compounds has greatly multiplied, leading to an increased interest in microfluidics. Total integration of the detector and pump are necessary to decrease the overall size of the microfluidic device. Using previously developed thin film technologies, an electroosmotic flow (EOF) pump was incorporated in a microfluidic liquid chromatography device. An EOF pump was chosen because of its simple design and small size. EOF pumps fabricated on silicon and glass substrates were evaluated. The experimental flow rates were 0.19-2.30 μL/min for 40-400 V. The theoretical pump efficiency was calculated along with the generated mechanical power by various pump shapes to elucidate more efficient pump designs.

To better understand the EOF on plasma enhanced chemical vapor deposition (PECVD) silicon dioxide, the zeta potential was investigated. PECVD oxide is amorphous and less dense than thermal silicon dioxide, which slightly changes the zeta potential. Zeta potentials were found for pH values from 2.6 to 8.3. Also, surface defects that affect the zeta potential were observed, and procedures to detect and prevent such defects were proposed.

Finally, surface modifications to the microfluidic device were attempted to demonstrate that thin film EOF pumps can be used in the liquid chromatographic separation of mixtures. The microfluidic separation channel was coated with chlorodimethyloctadecylsilane, however, due to problems with channel filling and reservoir adhesives, separation was not achieved. The use of new adhesives and external pumps were proposed to resolve these problems for future testing. Also new methods to combine EOF pumps with microfluidic channels and on-chip detectors were suggested.

ACKNOWLEDGEMENTS

I would like to express my gratitude to Dr. Milton L. Lee for allowing me to be a member of his research group. During the two and a half years that I have been here, I have greatly benefited from Dr. Lee's advice, knowledge, and encouragement. I would also like to thank my graduate committee members, Dr. Hawkins, Dr. Linford and Dr. Woolley, for their advice, and help with my project. I am also indebted to Mark Hamblin, Megan Larsen and Yan Fang for their assistance in my project. I am very grateful to have had great lab mates in chemistry and electrical engineering such as Jesse Contreras, Jacoline Murray, Yuanyuan Li, Nosa Agbonkonkon, Jikun Liu, Jenny Armenta, Evan Lunt, John Hulbert, Matt Holmes and many others.

I would like to thank my parents, John and Dawnella Edwards, for all the support and encouragement they have given me. Finally, I would like to express my appreciation to the Department of Chemistry and Biochemistry at Brigham Young University for allowing me to study here and for the financial support I received from the Department and from the National Institutes of Health.

TABLE OF CONTENTS

LIST OF FIGURES

1 INTRODUCTION

1.1 Rationale and Motivation

Chromatography has grown into the most important analytical method for separating and identifying compounds in mixtures. Chromatography's versatility has been important for pharmaceuticals, forensics, environmental studies and many others. The number of applications utilizing chromatography are numerous and always increasing. There is an ever increasing demand for improving chromatographic techniques and using them in new applications. During the early 1990's, an approach to improve analysis was the creation of miniaturized total chemical analysis systems (μTAS).[1-3] Benefits of μTAS include reducing consumption of analytes, reagents and fluidic media. Since its early roots, research in microfluidics has become popular in separation science due to the ability to integrate an entire separation system within a miniaturized real estate platform.

1.2 History of Microfluidic Devices

μTAS developments have been progressing in several different areas. Some of the earliest research in micromachining was done by Terry *et al*.[4] in 1979, who attempted to create a miniaturized gas chromatograph. In 1977, IBM reported miniaturized ink jet nozzles fabricated on silicon.[5] Micromachined devices have come in many different forms ranging from simple devices such as valves to more complex devices which employ pumps, sensors, separation systems, etc. Most micromachining used in microfluidics is based on technology developed by the semiconductor industry, where line width dimensions are in the sub-micrometer range. This allows for smaller device dimensions.[6] The original enticement to use μTAS was that they allowed increased

chemical sensitivity over devices of the period that could not provide the desired selectivity and lifetime.[6] Furthermore, μTAS devices potentially could be further reduced to create portable hand-held devices that are capable of analyzing complex samples. One of the main objectives of microfluidics is the creation of miniaturized devices that can give laboratory-quality data in a non-laboratory atmosphere. Currently, many research groups are attempting to create portable detection systems that can be used in military applications, homeland security, medical offices and many other areas where small size analyzers are preferable.[7] Miniaturized devices can provide accurate preliminary results about a patient's condition, reducing the analysis time spent by an independent lab.[7] There are also many environmental applications where analyses need to be performed to detect sample contamination. Another benefit of size reduction is the ability to replace parts at lower cost and store multiple replacements in a small space.[6] The only size limitations at this point are the associated detection system and fluid pump.

1.3 Miniaturization of Pumps

Pumps have been made in all shapes and sizes. Each pump has been made to optimize the current technology, specific need and size. In many cases, the most important considerations have been size, power consumption and cost.[8] Over the last couple of decades, pumps have tended toward smaller sizes and more powerful systems. Wego *et al.*[11] in 2001 created a 780 mm^3 thermo-pneumatic pump. Schabmueller *et al.*[9] in 2002 created a 120 mm^3 single-chamber reciprocating displacement micropump. In 1995 Zengerle *et al.*[10] made an electrostatic pump with dimensions of 98 mm^3. With each type of pump, great strides have been taken to decrease pump dimensions.

1.4 Types of Pumps

There are many different types of pumps, all of which fall into two categories: reciprocating and continuous-flow pumps. For reciprocating pumps, pressure is generated by periodically compressing and expanding a fluid volume using moving surfaces within the pump. Electromagnetic, piezoelectric, thermopneumatic and electrostatic pumps are examples of reciprocating pumps. Reciprocating pumps produce the highest pressures and are the most commonly used. However, they produce pulse-like fluid flows and are usually very intricate.[8] Dynamic pumps, in contrast, generate pressure as the fluid gains momentum while traveling through the pump. Some common dynamic pumps include electroosmotic, magnetohydrodynamic and ultrasonic pumps. These pumps provide constant, pulse-less flow, require fewer parts and can be made much smaller than reciprocating pumps.[8]

Out of the many types of pumps available, electroosmotic flow (EOF) pumps are particularly attractive as alternatives to conventional pumping systems because of their smaller size and absence of moving mechanical parts. EOF pumps are attractive as pumps in μTAS because they employ EOF to sharpen peak profiles and eliminate the need of an external pump. Small EOF pumps are desirable for fluid delivery for flow injection analysis, capillary electrochromatography, lab on a chip, etc.[12-14] EOF pumps are the simplest type of pump that can be integrated and used in CE. Electrically driven pumps are also advantageous because they provide pulse-free, plug-like profiles, eliminating any velocity differential that is created as the fluid approaches the channel walls[15,16] until after the flow leaves the pump.

1.5 EOF Pump History and Theory

1.5.1 Introduction to EOF Pumps

Electroosmotic pumps have been around for several decades,[17,18] and theoretical models[16,19] have described flow rates and pressures that could be generated using such pumps. EOF pumps are known to work best for very small geographic areas, although larger pumps, which can generate higher pressures, could be implemented with current instruments. Pretorius *et al*.[18] were the first to use EOF as a pumping technique for injection systems. EOF pumps were not revisited until the 1990's when the move towards miniaturization and microfluidics gained increasing interest.[13]

1.5.2 EOF theory

EOF is the flow of fluid over immobile surface charges induced by an electric field.[15,20,21] Silicon dioxide, like most surfaces, contains negative surface charges formed by the ionization of the surface and the adsorption of ionic species. A layer of cations are attracted to the surface, maintaining a charge balance, which is called an electric double layer (EDL). Several different theories have been proposed to calculate the EDL thickness.[15,19,21] The simplest method to calculate the EDL thickness is to use the Helmholtz double layer approximation.[21] The Helmholtz double layer theory approximates the situation where the surface charge attracts counterions, neutralizing the charge a distance, *d*, from the surface. The surface charge potential is linearly dissipated from the surface to the counterions satisfying the charge. The radius of the counterions is approximately the distance, *d*. The Helmholtz model is overly simplistic and treats the counterion layer as though it were rigid.

Another method is the Gouy-Chapman model which suggests that the interfacial potential on a charged surface is attributed to the number of ions on the surface of one charge, and to an equal number of oppositely charged ions in the solution.[21,22] Unlike the Helmholtz double layer model, counter ions in the solution are not rigidly held to the surface and can diffuse into the solution. The distance that the counterions can diffuse into the solution is restricted by the counter potential from their departure. Double layer thickness is dependent on the kinetic energy of the counter ions.[21] The change in concentration of the counter ions, n, from the surface can be calculated using the Boltzman distribution, volume charge density, ρ, and the Poisson equation,[15,19]

$$n = n_o e^{-\frac{ze\psi}{kT}} \tag{1.1}$$

$$\rho = \Sigma zen \tag{1.2}$$

$$\frac{d^2\psi}{dx^2} = -\frac{4\pi\rho}{d} \tag{1.3}$$

where n_o is the bulk concentration, z is the charge of the ion, e is the charge on a proton and k is the Boltzman constant. The range Ψ varies from surface, Ψ_o, to 0 in bulk solution. Using Equations 1.1, 1.2 and 1.3 the double layer thickness, λ, can be derived resulting in Equation 1.4,[15,19]

$$\lambda = \left[\varepsilon_r kT /(4\pi e^2 \Sigma n z^2\right]^{1/2} \tag{1.4}$$

The Gouy-Chapman theory states that oppositely charged ions decrease in concentration with distance from the surface.[15,22] However, experimentally, the double layer thickness is usually greater than the calculated thickness.[20] Several assumptions may lead to this error. First, the activity is assumed to equal the molar concentration.[21] In solution, both anions and cations exist and there is a high probability that ions with the same

charge as the surface are found in the double layer increasing with distance from the surface.[21] Other false assumptions made are that ions act like point charges and that there are no physical limitations to the surface.[21] To correct for this, the Gouy-Chapman-Stern model was developed.[15] In the Gouy-Chapman-Stern model, ions have finite sizes, and cannot approach the surface within much less than a few nm.[22] This distance, δ, is about the length of the ion's radius. The ions can now be treated as point charges because of the lower potential and concentration of the diffuse part of the layer. Another assumption made in the Stern model is that some of the ions are adsorbed in the plane at a distance δ from the surface, forming what is called the Stern layer.

The third method to approximate the EDL is the Debye-Huckel approximation. Equation 1.5 is the Debye-Huckel approximation for the length of the double layer as,

$$\lambda = \frac{\left(\varepsilon_e RT\right)^{1/2}}{F\left(\Sigma z_i^2 c_i\right)^{1/2}} \tag{1.5}$$

where F is the Faraday constant, ε_e is the electrical permittivity, c_i is the concentration of the electrolyte and z_i is the valence of species i.[23] The EDL thickness is approximately the Debye length in the solution and is determined by thermal diffusion and electrostatic interactions.[16,22,24] The Debye-Huckel approximation works best at low ionic concentrations and voltages. At higher ionic concentrations and voltages, the Gouy-Chapman-Stern method is more appropriate.[16,22]

Ionic bonding of cations to the surface creates a potential difference known as the zeta potential. With the application of an electric field to the solution, ions travel with respect to the field, even when they are attracted to the opposite electrode. With the cation movement to the cathode, the bulk of the solution is dragged with it. The

movement of the fluid induces pressure and fluid movement to other locations. The flow produced by the attraction of the cations to the cathode and the bulk movement of the solution results in a plug-like profile.

1.5.3 Packed and Open Tubular Columns

Capillary columns used for EOF pumps are made from either packed or open tubular channels. Induced pressure is a function of surface area. Therefore, packed-channel EOF pumps produce higher pressures than open-channel EOF pumps at much lower currents.[25-28] In experiments done by Tripp *et al.*[17] using polymer monoliths, EOF pumps were capable of producing pressures of 55.1 psi and flow rates of 41 mL/min at 50 V. Other experiments done by Chen *et al.*[14] using silica particles in EOF pumps produced pump pressures of 2895 psi with flow rates of 1.6 mL/min at 28 kV. These are much higher pressures than those achievable with an open tubular column. One open tubular pump produced 4.79 psi and a flow rate of 0.015 mL/min at 1 kV.[29] As Chen *et al.*[14] and Tripp *et al.*[17] demonstrated, packed and monolithic EOF pumps are capable of generating higher pressures than open tubular EOF pumps. Maintaining particle diameter, monolith structure and packing density are significant drawbacks to packed and monolithic columns.[25-27] The first problem is that inconsistencies in the particles and monolith affect the surrounding fluid velocities in specific regions in the column/channel.[25] When electric double layers overlap, surrounding fluid velocity decreases.[20] Another problem with inconsistencies in the monolithic and packed columns is that each device or column will be slightly different from each other which can make data reproducibility difficult.[30] However, in each of the afore mentioned experiments EOF measurements were taken in silica capillaries as opposed to channels

on a silicon die.[14,17,29] It is much more difficult to gain channel access and insert packing material or develope a monolith in a microfabricated device than in a silica capillary. Therefore, it is much easier to use an open tubular channel; there are fewer processing steps needed and particle and pore diameter consistency concerns are eliminated. For these reasons, open tubular channels have been used for this work.

1.5.4 Purpose of EOF Pumps

EOF pumps are attractive when separation channel surfaces are functionalized with non-polar stationary phases.[24] When a reverse phase is used in a microchannel, the electric double layer is not able to form over the surface and the mobility is greatly reduced between the electrodes.[24] The only way to move liquids through the channel is with the incorporation of a pump. But as has been stated before, pumps are bulky and often expensive. However, by incorporating a smaller pump such as an EOF pump, the size of the μTAS system is not greatly increased. Besides generating fluid flow over a reversed phase coating, EOF pumps can also be used to pump liquids through packed capillary channels. While plug flow is generated in the pump itself, the flow profile becomes more parabolic, which is observed with other types of pumps (i.e., reciprocating pumps), when the liquid enters the separation channel/column.

1.6 Electrically Driven Separations

1.6.1 Types of Fluid Flow

Capillary electrophoresis is an important analytical method often used in clinical laboratories to analyze proteins, carbohydrates, peptides, drug metabolites and many other molecules.[31] There are six common modes of capillary electrophoresis including capillary isoelectric focusing (CIEF), capillary zone electrophoresis (CZE), capillary

electrochromatography (CEC), capillary isotachophoresis (CITP), capillary gel electrophoresis (CGE), and micellar electrokinetic chromatography (MEKC). In each of these modes, analyte separation occurs because of an applied voltage rather than an applied pressure like most other forms of chromatography. In CEC separations, two types of electrokinetic forces are used. The first is electrophoresis and the second is electroosmosis. Depending on the experiment, electroosmosis is undesirable and it can be reduced or eliminated by adding surface coatings or buffer additives.

1.6.2 Electrophoretic Theory

Electrophoresis is the movement of charged ions or molecules when influenced by an external electric field. Cations and anions are separated with cations attracted to the cathode and anions to the anode. Electrophoresis is due to the Lorentz force which is related to the charge of the ions or molecules and the electric field. Lorentz forces are equal to the ion charge, q, and the potential gradient, E, which is expressed in Equation 1.6. The potential gradient is equal to the applied voltage divided by the distance between the two electrodes,

$$F_e = qE \tag{1.6}$$

$$F_f = vf \tag{1.7}$$

Equation 1.7 is the frictional force, where v is the velocity and f is the frictional coefficient. Electrical force promotes motion and frictional forces act against motion. The frictional force is affected by the buffer viscosity, molecule shape, surface, and hydrodynamic size of the molecule. The electrophoretic mobility, μ, depends on solution and particle properties. The simplest way to calculate the mobility is by setting the frictional force equal to the Lorentz force,

$$\mu_{ep} = \frac{v}{E} = \frac{q}{f} \tag{1.8}$$

This equation is true when the ion concentration is approximately 0 and the solution is nonconductive.[32,33] As was shown with electroosmosis, ions are surrounded by counterions of that species to help form neutrality which alters the mobility. This simplified form also neglects to look at the particles and solution properties. Some of the important particle properties include the surface charge density and size, which determine the separation of the analytes.[32,33] Important solution properties include electric permittivity, ionic strength and pH.[16] The electrophoretic mobility can be approximated by the Smoluchowski equation,

$$\mu_{ep} = \frac{\varepsilon\varepsilon_o\zeta}{\eta} \tag{1.9}$$

where ζ is the surface potential or zeta potential of the particle, ε is the dielectric constant of the liquid, ε_o is the permittivity of free space, and η is the viscosity of the liquid.

1.6.3 Separations Involving Electroosmosis and Electrophoresis

Electrophoresis separates primarily according to charge and size. Molecules with similar charges are separated by different frictional forces due to their sizes.[32,33] Each type of molecule travels at a different rate depending on its charge and attraction to the electrode.[32,33] Therefore, ions with greater charge and smaller size move faster. Electrophoretic velocity can be changed by changing the solution (which changes the friction force), changing the pH to affect the charge and by changing the potential gradient. Electrophoresis is advantageous for separations because the electrophoretic mobility is constant at the same voltage.[34] The movement of analytes can occur at different rates depending on surface-analyte interactions.[35]

Electroosmosis is bulk flow movement of the solution through the channel. Unlike electrophoresis where the ions are the only moving species, in electroosmosis, neutral analytes also move. Electroosmosis is at a maximum in silica channels when the pH is greater than 9 because most silanol groups are ionized, and it is the lowest when the pH is below 2.4 because most silanol groups are protonated. The EOF mobility is primarily affected by the buffer viscosity, zeta potential, surface area of the channel, and dielectric constant.[36] Due to the plug-like flow of the solution analytes separate into narrow bands.

For separations using both electrophoresis and electroosmosis, the observed electrophoretic mobility, μ_{obs}, can be found by adding the electrophoretic mobility, μ_{ep}, and the electroosmotic mobility, μ_{eof}, as seen in Equation 1.10,

$$\mu_{obs} = \mu_{ep} + \mu_{eof} \tag{1.10}$$

The EOF travels from the anode to the cathode dragging the solution with it, for silicon dioxide surfaces at pH greater than 2.4. As the EOF travels towards the cathode, the cations have a positive μ_{ep}, the anions have a negative μ_{ep}, and the neutral species have a μ_{ep} of 0. By having all compounds travel in the same direction, this eliminates the need for a second detector at the other electrode and it causes neutral compounds, which otherwise do not move, to travel to the detector. Analyte bands have a plug-like profile as they separate because of the plug-like EOF flow which in turn increases peak capacity and resolution. Separations only using electrophoresis are best when the charges of the analytes are quite different and the number of analytes to be detected are limited. CZE separation is the most common CE method using both electrophoresis and electroosmosis. By incorporating a non-polar surface coating or packing into a section

of a device containing an EOF pump, a hybrid separation method for both CZE and CEC is created.[37] This method has the advantage of using electroosmotic and electrophoretic mobilities to separate analytes across the region of the device that does not contain the non-polar coating. Then by using the EOF to pump the mobile phase through the non-polar section of the device, the analytes are further separated according to their differences in affinity to the non-polar surface.[37]

1.7 Chip vs. Polymer/Glass Bonding

Both inorganic and organic materials, are used to form CE devices. However, most miniaturized CE devices are made on glass or polymeric substrates. Glass and some polymer substrates are ideal because they are transparent, which is essential since laser-induced fluorescence (LIF) is commonly used to detect the separated analytes.[6] However, horizontal detection through microchannels made of thin silicon dioxide or nitride layers on a silicon substrate allow for new strides to be made with silicon as a substrate, even though breakdown voltages for these types of devices are low. By using silicon dioxide and silicon nitride coatings, electric fields comparable to those used in other CE devices can be used with silicon substrates.[38]

1.7.1 Inorganic Substrates

Inorganic substrates are prepared by thoroughly cleaning the surfaces in mixtures such as H_2SO_4/H_2O_2 and HF.[38] There are many methods to prepare CE channels in inorganic substrates, but most use photolithographic techniques developed for the semiconductor industry. Typically, a layer of photoresist (a polymer that chemically changes when exposed to ultraviolet (UV) radiation) is spin coated on top of the surface. Next, the photoresist is patterned by placing a high resolution photomask on top of the

photoresist and exposing it to UV light. Depending on the type of photoresist, either the exposed region (positive photoresist) or the unexposed region (negative photoresist) is dissolved in the developing solution. After the photoresist is patterned and developed, the uncovered regions of the substrate can be chemically etched. Chemical etching falls into two categories: wet and dry etching. Dry etching is commonly done using reactive gases; an example is reactive ion etching (RIE).[39] After the channels in the substrate have been etched a second substrate, to close off the channel, is bonded to the first substrate. Dry etching requires more expensive and complicated instrumentation, but gives high aspect ratios (depth/width).

There are a variety of wet etchants that can be used depending on the substrate. For silicon, KOH is the most commonly used etchant; however, other etchants containing HF, HNO_3 and CH_3COOH are also used.[39,40] For glass, HF is the most commonly used etchant. Wet etching is cheaper and easier, but gives lower aspect ratios compared to dry etchants. After the substrate is etched to the desired depth, the photoresist is removed and the surface is cleaned again in H_2SO_4/H_2O_2. To create the microfluidic device, a second glass or silicon substrate with holes for the reservoirs is bonded on top of the etched region of the first substrate. Glass or silicon surfaces are chemically bonded using several different methods such as thermal, anodic, water glass solution, and electromagnetic radiation. In thermal bonding, substrates are bonded together by bringing the two surfaces together, applying pressure, and heating them to 500-700 ºC to form siloxane bonds between the silanol groups.[5] Thermal bonding requires high temperatures and very clean surfaces; otherwise weak bonds and channel morphing result.[41] One alternative to chemical bonding is to use adhesives.[42]

1.7.2 Organic Substrates

Alternatively, various polymers have been investigated as replacements for inorganic substrates. Some of the polymeric materials that have been considered include poly(methyl methacrylate) (PMMA),[43] polystyrene (PS),[44] polycarbonate (PC),[45] polyethylene terephthalate (PET)[46] and polydimethylsiloxane (PDMS).[47] Due to the diversity of polymers that can be used, there are a variety of methods for fabrication which fall into two categories: replication and direct methods.

Replication methods entail using a template to create the microchannel features. The template is typically made from a hard material such as metal,[39] silicon,[48] or hard polymers such as polyetheretherketone (PEEK).[49] Metal templates for microfluidic devices are usually made using a silicon substrate that has been fashioned using the same photolithography techniques described earlier in section 1.7.1. Once the substrate has been made, a metal or seed layer is evaporated or sputtered onto the silicon surface. Then a thicker metal layer is grown on top of the seed layer by electroplating. After the metal template is created, the silicon substrate is removed by etching away the silicon in a KOH solution.[39] For silicon templates, the same type of photolithographic methods used to make the silicon substrate are used to make the template. Once the template is made, the microfluidic device can be made. Hot embossing is the most commonly used technique to fabricate polymer microfluidic devices for thermoplastics such as PET, PS, PC and PMMA.[48] During hot embossing, the polymeric substrate is heated past its glass transition temperature (T_g) and brought into contact with the template. The template and substrate are embossed using pressure and then cooled to just below the T_g to release the template. Another replication method used is injection molding. In injection

molding, polymer pellets are melted to form a liquid which is then injected into a mold that contains the template.[49] Casting is the easiest of the three replication methods.[50] In casting, a liquid polymer, typically PDMS, and a curing agent are poured into a mold containing the template and then cured.

Laser micromachining is the most commonly used direct method to make microfluidic devices. Typically, a CO_2 or UV excimer laser is used to ablate the pattern into the polymeric substrate.[51] Sometimes the ablation process creates deformed channels due to excessive heating during the process. Other problems include re-deposition of polymer residues or decomposed compounds which change the surface properties of the device.[51]

There are several common methods of bonding a patterned substrate to a blank substrate to enclose the microfluidic channels.[43,44] Thermal bonding is the most commonly used method for bonding substrates together. In this case, the substrates are heated to just above the T_g of the polymer and pressed together to physically bond. Solvent bonding is another commonly used technique to bond polymer substrates by using organic solvents to partially dissolve the polymer chains at the surfaces of the substrate.[39] Once the polymer chains are partially dissolved, they can be bonded to each other when compressed. Adhesives can also be used to bond two substrates together, however, care must be taken to prevent adhesive glues from entering the microchannels.[52]

Most research using fabricated microfluidic devices is done on polymeric or glass substrates.[43-49] Glass devices require more time to fabricate and are harder to mass produce than polymeric devices. However, glass devices are typically better for high-performance and fast separations. Also glass has better optical thermal properties.[38,42-49]

Polymer substrates have greatly improved what is known and can be done with miniaturized CE methods, but the ultimate goal of a "lab on a chip" cannot be fully realized until the detector and pump are integrated with the separation device, rather than being external components. Incorporating microchip components for the detector on the least amount of real estate could best be done on a silicon substrate, even though the cost of the device may be expensive. However, silicon is semi-metallic it conducts current better than commonly used solutions in CE, which makes silicon devices hard to use in CE separations. However, the solution to this problem lies within a technology called thin film deposition.[38] Oxide layers can be deposited on top of a silicon substrate containing microchip components. This allows for higher voltages up to 2000 V, depending on the thin film deposition thickness, to be used since an insulating layer is now the channel region with which the fluids come in contact.[53] Using thin films allows for the potential integration of electronic circuits with a CE device, leaving the pump as the final component to integrate. As mentioned earlier, EOF pumps are "built-in" pumps that use the naturally occurring phenomenon of electroosmotic flow, and eliminate the need for an external pump.

1.8 Thin Film Fabrication

Thin film fabrication of microchannels follows well established methods developed for the semiconductor industry. In adaptation of earlier thin film processing,[38,54,55,56] EOF pumps were fabricated on silicon and glass wafers (Fig. 1.1). A 2.5-μm layer of thermal silicon dioxide was grown to prevent electrical breakdown of the silicon substrate. A 200-nm layer of silicon nitride was deposited by plasma enhanced chemical vapor deposition (PECVD) to act as an etch stop layer. An additional

300 nm of silicon dioxide were deposited by PECVD to form the bottom layer of the microchannels. This same oxide layer was also deposited on top of the glass wafers to give the same surface consistency to each microchannel. Next the sacrificial layer was made from aluminum and photoresist by evaporating 300 nm of aluminum on the wafer followed by a spin coated layer of 3 μm AZ3330 photoresist (AZ Clariant, Somerville, NJ). Next, the photoresist was patterned with the microchannel design and developed in AZ 300 MIF developer (AZ Electronic Materials, Somerville, NJ). After the photoresist was patterned, the features were rectangular in shape; however, to give the channels a rounded shape, the photoresist was heated to 250 °C to reflow it. Finally, the aluminum was etched with an aluminum etchant (Transene, Danvers, MA). Once the sacrificial layer was completed, 3 μm of PECVD silicon dioxide is deposited on top of the wafer. To etch the sacrificial layer, the channel ends were opened by coating the wafer with a second layer of photoresist which was exposed and developed. The photoresist layer protected everything but the channel ends, which were now etched with buffered hydrofluoric acid (Transene). The aluminum was first removed by submerging the wafer in 2:1 HCl/HNO_3. Following removal of the aluminum layer, the photoresist layer was removed using Nanostrip (Cyantek, Fremont, CA). The final dimensions of the microfluidic features were 5 μm wide and 4 mm long for the smaller pump channels, and 50 μm wide and 5 mm long for the wider channel.

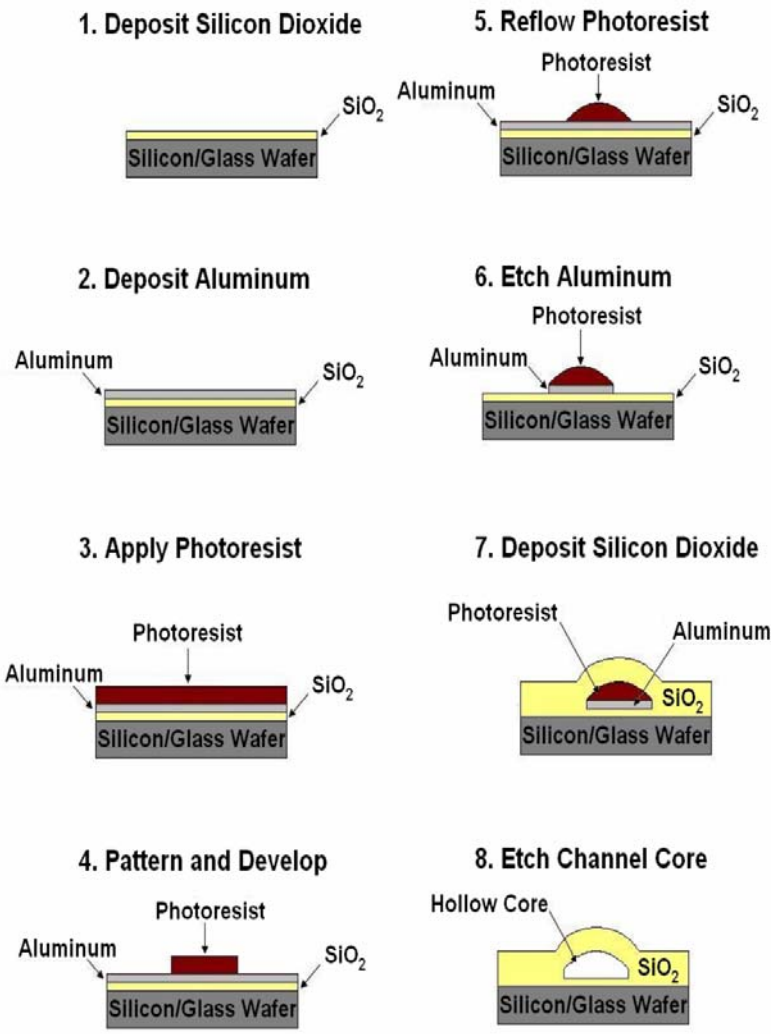

Figure 1.1 Thin film fabrication process used to create microchannels.[53]

1.9 Thin Film Surfaces

Thin film deposition using PECVD is one approach to creating silicon dioxide surfaces.[36,57-60] Silicon dioxide can also be thermally grown, which required high temperatures up to 1200 ºC.[61] These high temperatures do not allow for organic or metallic layers. By using a plasma, much lower temperatures are required than thermally grown silicon dioxide layers, because the plasma causes the individual molecules to reach temperatures up to 21,000 K, while the actual temperature of the system is much lower (usually 200-400 ºC).[59,60] In PECVD, the high temperature reduces the ΔG of the reaction, making the reaction more favorable.[59,60] PECVD involves the excitation of gases which react to form layers on the surface. These layers adhere to the surface by chemical bonds and physical adhesion. The physical adhesion of thin film to the surface is relatively weak, whereas the chemical bonds, van der Waals' forces and sometimes covalent bonds, are much stronger. When ions bombard the surface, they increase the surface defect density, improving the binding energy.[59] CVD films are amorphous with bond-like polymer chains forming occasional covalent bonds with the surface below.[59,60] Plasmas produce five different chemical processes: excitation, ionization, relaxation, dissociation and recombination.[59] The gases I used to create the oxide layer are silane (SiH_4) and nitrous oxide (NO_2). They react as follows,

$$SiH_4 + 2NO_2 \rightarrow SiO_2 + 2H_2O + N_2 \qquad (1.11)$$

This equation describes stoichiometrically what happens; however, due to the complexity of plasma reactions, there are often multiple different products. Often, there is residual hydrogen in the film. Experimentally, it has been found that this hydrogen content contributes to stresses in the film and a lower density than crystalline silicon dioxide.[59,60]

The stresses in the thin film are in the plane of the film.[59,60] Therefore, these stresses are greatest at the edges. Stresses in the film reduce adhesion and increase the chances of cracking. Typically, to reduce stress and hydrogen content, the films are thermally annealed between 400-600 °C.[59,60] This has been shown to help strengthen the thin film, but sometimes the optical properties of the film are compromised.

1.10 Coated and Uncoated Surfaces

The surfaces of most microfluidic devices produce undesirable analyte adsorption due to nonspecific interactions such as hydrogen bonding, and electrostatic and hydrophilic interactions between the analyte and the surface.[62] Protein adhesion depends on protein affinity to the surface, ionic strength and nature of the salts in the solution, and the new protein structure formed on the surface.[35,36] Surface adsorption slightly changes the zeta potential of the microfluidic device, ultimately changing the EOF.[34,36] This results in skewed peaks and loss in analytical reproducibility in CEC. Another problem is that proteins may denature on the surface.[36] To resolve these problems, surface coatings are often used to reduce analyte adhesion. Surface coatings can be neutral, positive, or negatively charged moieties or cross-linked polymers. Surface coatings can also be employed to stop or reduce EOF and to change the separation speed and sometimes the direction of the separation.[34] Surface coatings fall into two categories: permanent and temporary (dynamic).

Temporary or dynamic coatings are simple and easy to apply to a device surface. Dynamic coatings involve physical interactions of the coating with the surface prior to introduction of the analyte. There are a wide variety of surface coatings that are available, including compounds such as poly(ethylene oxide) (PEO),[63] poly(vinyl

alcohol)[64] and polymer bilayers made of polybrene (PB) and dextran sulfate (DS).[65,66] For dynamic coatings to be effective, the coating must be reapplied occasionally to ensure complete coverage. Dynamic coatings can interfere with detection such as mass spectrometry. Also dynamic coatings can sometimes denature proteins, so specific coatings must be used for different analytes.

Permanent surface coatings chemically modify and bond covalently with the surface and do not need to be constantly replaced. Most permanent coatings are polymers or silane reagents such as octadecyltrimethoxysilane (ODMS),[67,68] polyethylene glycol (PEG),[68] polyacrylamide,[69,70] 3-glycidoxypropyltrimethoxysilane (GPTMS),[69] poly(vinylpyrrolidone)[70] and many others. The major concern with using permanent coatings is the lifetime of the coating, which makes dynamic coatings attractive because they can be more easily renewed.[36] The more hydrophobic the coating, the better protected is the silica from hydrophilic proteins.[71] Another advantage of permanent coatings is the wide range of materials that are available, which can be selected for specific analytes.[72] Permanent coatings can also be used to coat specific regions of a device.

1.11 Overview of this Thesis

Chapters 2 and 3 present the fabrication and evaluation of electroosmotic pumps that were incorporated into thin film microfluidic devices. Chapter 2 describes the thin film fabrication method used to create the electroosmotic pumps and the EOF flow rates attainable from this type of pump. This chapter also describes designs for improved pumps. In Chapter 3, surfaces of the silicon dioxide thin films are described in terms of the zeta potential, and in the quality and testing of thin film channels. This chapter also

discusses how to better control surface quality and procedures to determine device quality. In Chapter 4, experiments that have been done to incorporate a surface coating in a thin film microchannel are discussed and ways to improve this technique are postulated. Finally, in Chapter 5, conclusions and future work are discussed.

1.12 References

1. Harrison, D. J.; Manz, A.; Fan, Z.; Ludi, H.; Widmer, M. *Anal. Chem*. **1992**, *64*, 1926-1932.
2. Manz, A.; Miyahara, Y.; Miura, J.; Watanabe, Y.; Miyagi, H.; Sato, K. *Sens. Actuators* **1990,** *B1*, 249-255.
3. Manz, A.; Graber, N.; Widmer, H. M. *Sens. Actuators* **1990**, *B1*, 244-248.
4. Terry, S. C.; Jerman, J. H.; Angel, J. B. *IEEE Trans. Electron Devices* **1979**, *26*, 1880-1887.
5. Bassous, E.; Taub, H. H.; Kuhn, L. *Appl. Phys. Lett.* ***1977***, *31*, 135-137.
6. Reyes, D. R; Iossifidis, D.; Auroux, P-A. ; Manz, A. *Anal. Chem*. **2002**, *74*, 2623-2636.
7. Takats, Z.; Wiseman, J. M.; Cooks, R. G. *J. Mass Spec.* **2005**, *40*, 1261-1275.
8. Laser, D. J.; Santiago, J. G. *J. Micromech. Microeng*. **2004**, *14*, R35–R64.
9. Wego, A.; Pagel, L. *Sens. Actuators A* **2001**, *88*, 220-226.
10. Schabmueller, C. G. J.; Koch, M. ; Mokhtari, M. E. ; Evans, A. G. R.; Brunnschweiler, A. Sehr, H. *J. Micromech. Microeng*. **2002**, *12*, 420-424.
11. Zengerle, R.; Ulrich, J.; Kluge, S.; Richter, M.; Richter, A. *Sens. Actuators A* **1995**, *50*, 81-86.
12. Liu, S.; Dasgupta, P. K. *Anal. Chim. Acta* **1992**, *268*, 1-6.
13. Dasgupta, P. K.; Liu, S. *Anal. Chem*. **1994**, *66*, 1792-1798.
14. Chen, L.; Ma, J.; Guan, Y. *J. Chromatogr. A* **2004**, *1028*, 219-226.
15. Ajdari, A. *Phys. Rev. E* **1996**, *53*, 4996-5005.
16. Santiago, J. G. *Anal. Chem.* **2001**, *73*, 2353-2365.

17. Tripp, J. A.; Svec, F.; Frechet, J. M. J.; Zeng, S.; Mikkelsen, J. C.; Santiago, J. G. *Sens. Actuators B* **2004**, *99*, 66-73.

18. Pretorius, V.; Hopkins, B. J.; Schieke, J. D. *J. Chromatogr*. **1974**, *99*, 23-30.

19. Rice, C. L.; Whitehead, R. *J. Phys. Chem*. **1965**, *69*, 4017-4024.

20. Grimes, B. A.; Liapis, A. I. *J. Colloid Interface Sci*. **2003**, *263*, 113-118.

21. Hiemenz, P. C.; Rajagopalan, R. Eds. Principles of Colloid and Surface Chemistry, Third Edition, Revised and Expanded, Marcel Dekker, New York, 1997.

22. Camilleri, P. Capillary Electrophoresis: Theory and Practice; CRC Press: Boca Raton, FL, 1993.

23. Conlisk, A. T.; McFerran, J.; Zheng, Z.; Hansford, D. *Anal. Chem*. **2002**, *74*, 2139-2150.

24. Dutta, P.; Beskok, A. *Anal. Chem*. **2001**, *73*, 1979-1986.

25. I. Nischang, I.; Chen, G.; Tallarek, U. *J. Chromatogr. A* **2006**, *1109*, 32-50.

26. Zeng, S.; Chen, C.; Mikkelsen Jr., J. C.; Santiago, J. G. *Sens. Actuators B*, **2001**, *79*, 107.

27. Paul, P. H.; Garguilo, M. G.; Rakestraw, D. J. *Anal. Chem*. **1998**, *70*, 2459-2467.

28. Wan, Q-H. *Anal. Chem*. **1997**, *69*, 361-363.

29. Chen, C-H; Santiago, J. G. *J. Microelectromech. Syst*. **2002**, *11*, 672-683.

30. Lazar, I. M.; Karger, B. L. *Anal. Chem*. **2002**, *74*, 6259-6268.

31. Manz, A. *Anal. Chem*. **1997**, *69*, 1200-1203.

32. Dolnik, V.; Hutterer, K. M. *Electrophoresis* **2001**, *22*, 4163-4178

33. Beale, S. C. *Anal. Chem*. **1998**, *70*, 279R-300R.

34. Xu, Y.; Takai, M.; Konno, T.; Ishihara, K. *Lab Chip* **2007**, *7*, 199-206.

35. Kuksenok, O.; Yeomans, J. M.; Balazs, A. C. *Langmuir* **2001**, *17*, 7186-7190.

36. Clicq, D.; Vervoort, N.; Vounckx, R.; Ottevaere, H.; Buijs, J.; Gooijer, C.; Ariese, F.; Baron, G. V.; Desmet, G. *J. Chromatogr. A* **2002**, *979*, 33-42.

37 Fujimoto, C.; Fujise, Y. *Anal. Chem*. **1996**, *68*, 2753-2757.

38. Barber, J. P.; Conkey, D. B.; Lee, J. R.; Hubbard, N. B.; Howell, L. L.; Schmidt, H.; Hawkins, A. R. *IEEE Photon. Technol. Lett*. **2005**, *17*, 363-365.

39. Griebel, A.; Rund, S.; Schonfeld, F; Dorner, W.; Konrad, R.; Hardt, S. *Lab Chip* **2004**, *4*, 18-23.

40. Kelly, R. T.; Woolley, A. T. *Anal. Chem*. **2003**, *75*, 1941-1945.

41. Bilitewski, U.; Genrich, M.; Kadow, S.; Mersal, G. *Anal. Bioanal. Chem.* **2003**, *377*, 556-569.

42. Wang, H. Y.; Foote, R. S.; Jacobsen, S. C.; Schneibel, J. H.; Ramsey, J. M. *Sens. Actuators B* **1997**, *45*, 199-207.

43. Soper, S.A.; Ford, S.M.; Xu, Y.; Qi, S.; Mcwhorter, S.; Lassiter, S.; Patterson, D.;Bruch, R.C. *J. Chromatogr. A* **1999**, *853*, 107-120.

44. Barker, S.L.R.; Ross, D.; Tarlov, M.J.; Gaitan, M.; Locascio, L.E. *Anal. Chem.* **2000**, *72*, 5925-5929.

45. Liu, Y.; Ganser, D.; Schneider, A.; Liu, R.; Grodzinski, P.; Kroutchinina, N. *Anal. Chem.* **2001**, *73*, 4196-4201.

46. Malmstadt, N.; Yager, P.; Hoffman, A.S.; Stayton, P.S. *Anal. Chem.* **2003**, *75*, 2943-2949.

47. McDonald, J.C.; Duffy, D.C.; Anderson, J.R.; Chiu, D.T.; Wu, H.K.; Schueller,

O.J.A.; Whitesides, G.M. *Electrophoresis* **2000**, *21*, 27-40.

48. Fu,G. C.; Fang, Z. L. *Anal. Chim. Acta* **2000**, *422*, 71-79.

49. Galloway, M.; Stryjewski, W.; Henry, A.; Ford, S. M.; Llopis, S.; McCarley, R. L.; Soper, S. A. *Anal. Chem*. **2002**, *74*, 2407-2415.

50. Whitesides, G. M.; Ostuni, E.; Takayama, S.; Jiang, X. Y.; Ingber, D. E. *Ann. Rev. Bio. Eng*. **2001**, *3*, 335-373.

51. Bowden, M. Geschke, O.; Kutter, J. P.; Diamond, D. *Lab Chip*, **2003**, *4*, 221-223.

52. Meng, Z.; Qi, S.; Soper, S. A.; Limbach, P. A. *Anal. Chem*. **2001**, *73*, 1286-1291.

53. Edwards IV, J. M.; Hamblin, M. N.; Fuentes, H. V.; Peeni, B. A.; Lee, M. L.; Woolley, A. T.; Hawkins, A. R. *Biomicrofluidics* **2007**, *1*, 014101-014111.

54. Barber, J. P.; Lunt, E. J.; George, Z. A.; Yin, D.; Schmidt, H.; Hawkins, A. R. *IEEE Photon. Technol. Lett*. **2006**, *18*, 28.

55. Peeni, B. A.; Conkey, D. B.; Barber, J. P.; Kelly, R. T.; Lee, M. L.; Woolley, A. T.; Hawkins, A. R. *Lab Chip* **2005**, *5*, 501-505.

56. Madou, M. J. *Fundamentals of Microfabrication*; CRC Press: Boca Raton, FL, 2002.

57. Huang, H.; Winchester, K. J.; Suvorova, A.; Lawn, B. R.; Liu, Y.; Hu, X. Z.; Dell, J. M.; Faraone, L. *Mater. Sci. Eng. A* **2006**, 453-459.

58. Han, S. S.; Ceiler, M.; Bidstrup, A.; Kohl, P.; May, G. *IEEE Trans. Comp. Packag., Manufact. Technol.* **1994**, *17*, 174-182.

59. Konuma, M. Plasma Techniques For Film Deposition. Alpha Science, Harrow, UK, 2005.

60. Sivaram, S. Chemical Vapor Deposition: Thermal and Plasma Deposition of Electronic Materials. Van Nostrand Reinhold, New York, 1995.

61. Van Zant, P. Microchip Fabrication, Fifth Edition, McGraw-Hill Professional Publishing Co., New York, 2004.

62. Ghosal, S. *Anal. Chem*. **2002**, *74*, 771-775.

63. Tseng, W. L.; Chang, H. T. *Anal. Chem*. **2001**, *72*, 2499-2506.

64. Gilges, M.; Kleemiss, M. H.; Schomburg, G. *Anal. Chem*. **1994**, *66*, 2038-2046.

65. Ro, K.W.; Chang, W.-J.; Kim, H.; Koo, Y.-M.; Hahn, J.-H. *Electrophoresis* **2003**, *24*, 3253-3259.

66. Liu, Y.; Fanguy, J.C.; Bledsoe, J.M.; Henry, C.S. *Anal. Chem.* **2000**, *72*, 5939-5944.

67. Kutter, J. P.; Jacobsen, S. C.; Matsubara, N.; Ramsey, J. M. *Anal. Chem*. **1998**, *70*, 3291-3297.

68. Zhao, Z.; Malik, A.; Lee, M. L. *Anal. Chem*. **1993**, *65*, 2747-52.

69. Hjerten, S. *J. Chromatogr*. **1985**, *347*, 191.

70. Huang, M.; Vorkink, W. P.; Lee, M. L. *J. Microcol. Sep*. **1992**, *4*, 233.

71. Jorgenson, J. W., Lukacs, K. D., *Science **1983***, *222*, 266–272.

72. Castelletti, L.; Verzola, B.; Gelfi, C.; Stoyanov, A.; Righetti, P. G. *J. Chromatogr. A* **2000**, *894*, 281-289.

2. THIN FILM ELECTROOSMOTIC PUMPS FOR BIOMICROFLUIDIC APPLICATIONS*

2.1 Introduction

With the continued application of micro-electromechanical systems (MEMS) in microfluidic applications, the demand for small, efficient, and easily fabricated fluid pumps is apparent. Micropumps fall into two general categories: reciprocating pumps and continuous flow pumps. Reciprocating pumps consist of an actuator, an inlet and outlet valve, and a pump chamber. Pressure is generated by moving surfaces in the pump that compress and expand periodically on a fluid. Common reciprocating micropumps include electromagnetic, thermopneumatic, piezoelectric, and electrostatic pumps. Reciprocating pumps are capable of high pressures, but are complex to build, and provide pulse-like fluid flows.[1] The second class of pumps, dynamic pumps, includes electroosmotic, electrokinetic, ultrasonic, and magnetohydrodynamic pumps. Pressure is generated in dynamic pumps from the momentum of a fluid as it moves through the pump. This type of pump provides constant, pulse-less flow, requires fewer parts and can be made much smaller than reciprocating pumps.[1] For these reasons, dynamic pumps are the most desirable for microfluidic devices, even though they cannot generate pressures as high as reciprocating pumps. This chapter describes a new electroosmosis-based dynamic pump.

Electroosmotic flow (EOF) is the flow of fluid over immobile surface charges induced by an electric field.[2,3] EOF starts with the formation of an electric double layer (EDL), which results as counterions are attracted to charges on a surface. The EDL

*This chapter is reproduced with permission from Biomicrofluidics 2007, 1, 014101-014105.

thickness is determined by electrostatic interaction and thermal diffusion, and approximates to the Debye length in the solution.[4] Once an electric field is applied to the solution, ions move with respect to the field, dragging the surrounding solution with them. EOF pumps take advantage of this fluid movement to induce pressure and total fluid movement for distribution to other locations in a fluidic network.

Electroosmosis as a pumping technique has been known for several decades.[5] Early on, research on EOF pumps was limited primarily to theoretical models. However, with increasing interest in small pumps for small volume fluidic manipulations, experiments involving EOF have greatly increased in number. Beginning with work done by Pretorius *et al*.[5] using packed silica particles in capillary columns, EOF pumps were shown to be adequate as pumps in fluid injection analysis systems. Other types of EOF pumps have been created in silicon and glass substrates either packed with silica or borosilicate glass particles,[6-10] or left open without any packing materials.[11]

EOF pumps are particularly attractive as alternatives to conventional pumping systems because of their small size and absence of moving mechanical parts. Small EOF pumps are desirable for fluid delivery for flow injection analysis, capillary electrochromatography, lab on a chip, etc.[12-14] EOF pumps fabricated directly on microchips instead of on bonded substrates decrease the overall size of the microfluidic system, are easier to integrate, and provide superior performance because of the reduction in connection fittings. Electrically driven pumps are also advantageous because they provide pulse-free, plug-like profiles in the flows generated in the pumps, eliminating any velocity differential that is created as the fluid approaches the channel walls[2,4] until after the flow leaves the pump. Previously fabricated EOF pumps have been shown to be

capable of generating very high pressures.[15] EOF pumps that are most commonly used in microchip separations are created by chemically etching channels in a glass substrate followed by thermally bonding a cover-plate with access holes over the etched channel pattern.

Packed channel EOF pumps have been shown to produce higher pressures than open channel EOF pumps at lower currents due to their increased surface area.[9,16,17] In experiments done by Tripp *et al*.,[15] polymer monoliths in EOF pumps were capable of producing pressures of 55.1 psi and flow rates of 0.41 mL/min at 50 V. Using silica particles in EOF pumps, Chen *et al*.[14] produced pump pressures of 2895 psi with flow rates of 1.6 μL/min at 28 kV. However, packing channels on a microchip is much more difficult than packing capillary columns. Packed and monolithic columns have the disadvantage that there are inconsistencies in particle diameter, monolith structure and packing density.[9,16,17] These inconsistencies affect the local fluid velocities at specific locations in the column/channel.[9] Overlapping electric double layers also contribute to a reduction in the surrounding fluid velocity. Open tubular capillary pumps are simpler to fabricate and give more reproducible results.[11]

In this chapter, the flow and pressure characteristics of open channel EOF pumps produced by thin film fabrication were investigated. From experimental flow rates, the pressures that were generated were determined. Theoretical calculations of pump efficiency were made to determine the optimum number of pump channels required to minimize chip space and electrical power.

2.2 Open Channel Pump Design

The open channel pump design consisted of multiple small channels connected to a large channel (Figure 2.1), as previously demonstrated by Lazar and Karger.[11] Our system setup differed in that we connected the electrodes to the ends of the multiple channel pump and single channel via two Teflon capillaries (see Figure 2.2). This was done due to the ease of electrode connection. This induced an EOF flow, although the contribution to the overall EOF flow was negligible when compared to that of the multichannel pump.

To further demonstrate the reasoning behind using multiple small channels versus a single large channel, the fluid flow and pressure generating properties of such configurations were examined. Lazar and Kager demonstrated the relationships shown in Equations 2.1 and 2.2 for EOF in an open capillary system,[11]

$$F_{eof} = \frac{\pi \varepsilon_o \varepsilon_r \zeta n d_1^2 E}{4\upsilon} \tag{2.1}$$

$$F_{\max} = \frac{F_{eof} \dfrac{L_1}{L_2}}{\dfrac{L_1}{L_2} + n\left(\dfrac{d_1}{d_2}\right)^4} \tag{2.2}$$

where n is the number of pump arms, ε_o is the electric permittivity of free space, ε_r is the relative permittivity of the fluid in the channels, ζ is the zeta potential of the channel walls, E is the electric field applied across the pump, L_1 is the length of the multi-channel pump segment, L_2 is the length of the microchannel attached to the EOF pump, d_1 is the

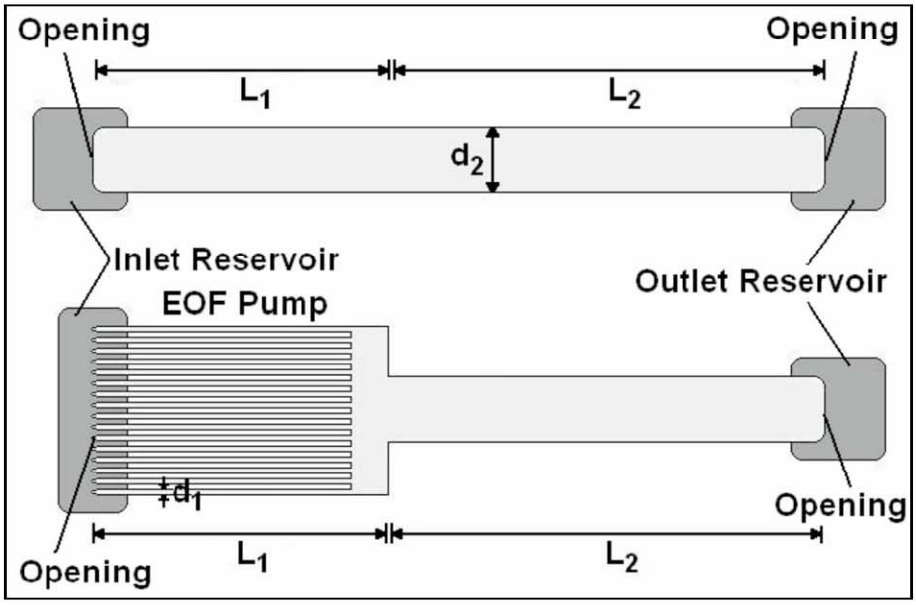

FIG. 2.1. Illustrations of EOF pumps consisting of (top) a single channel and (bottom) a single channel with multiple pump arms. Both have equal total cross-sectional areas.

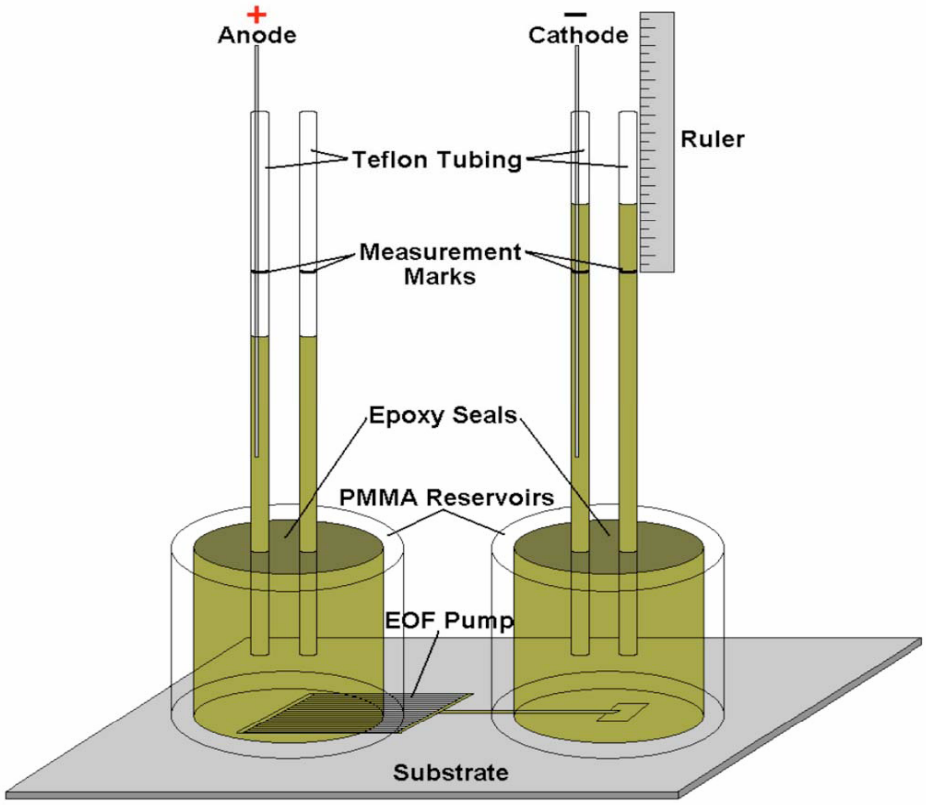

Figure 2.2. Schematic of the experimental setup for testing thin film EOF pumps.

equivalent diameter of one of the EOF pump arms, d_2 is the equivalent diameter of the microchannel attached to the EOF pump, and υ is the buffer viscosity.[11,18]

The maximum achievable flow was found by substituting Equation 2.1 into Equation 2.2 to produce Equation 2.3. The maximum achievable pressure was governed by Equation 2.4[11] as a function of the electric field,

$$F_{\max} = \frac{\pi n \varepsilon_o \varepsilon_r \zeta E L_1 d_1^2 d_2^4}{4\upsilon(L_1 d_2^4 + n L_2 d_1^4)} \tag{2.3}$$

$$\Delta P_{\max} = \frac{32 n \varepsilon_o \varepsilon_r \zeta E L_1 L_2 d_1^2}{L_1 d_2^4 + n L_2 d_1^4} \tag{2.4}$$

In this analysis, it was assumed that the sum of the cross-sectional areas of the EOF pump channels was equal to the cross-sectional area of the larger single channel. The length of the small channels in the multichannel EOF pump was designated L_1, and the larger channel was designated L_2. The single channel EOF pump, therefore, had a length of $L_1 + L_2$. Equation 2.5 gives the ratio of theoretical maximum flow rate generated by the multichannel EOF pump to the maximum flow rate generated by a single channel EOF pump of equal cross-sectional area.[11,18]

$$\frac{F_{multiple}}{F_{single}} = \frac{n(L_1 + L_2)}{(nL_1 + L_2)} \tag{2.5}$$

Figure 2.3 shows plots of Equation 2.5 as a function of small channel length (i.e., L_1) for different numbers of pump arms. The highest flow rates were found for short EOF pump lengths and high numbers of pump channels. This led to the EOF pump design shown in Figure 2.1.

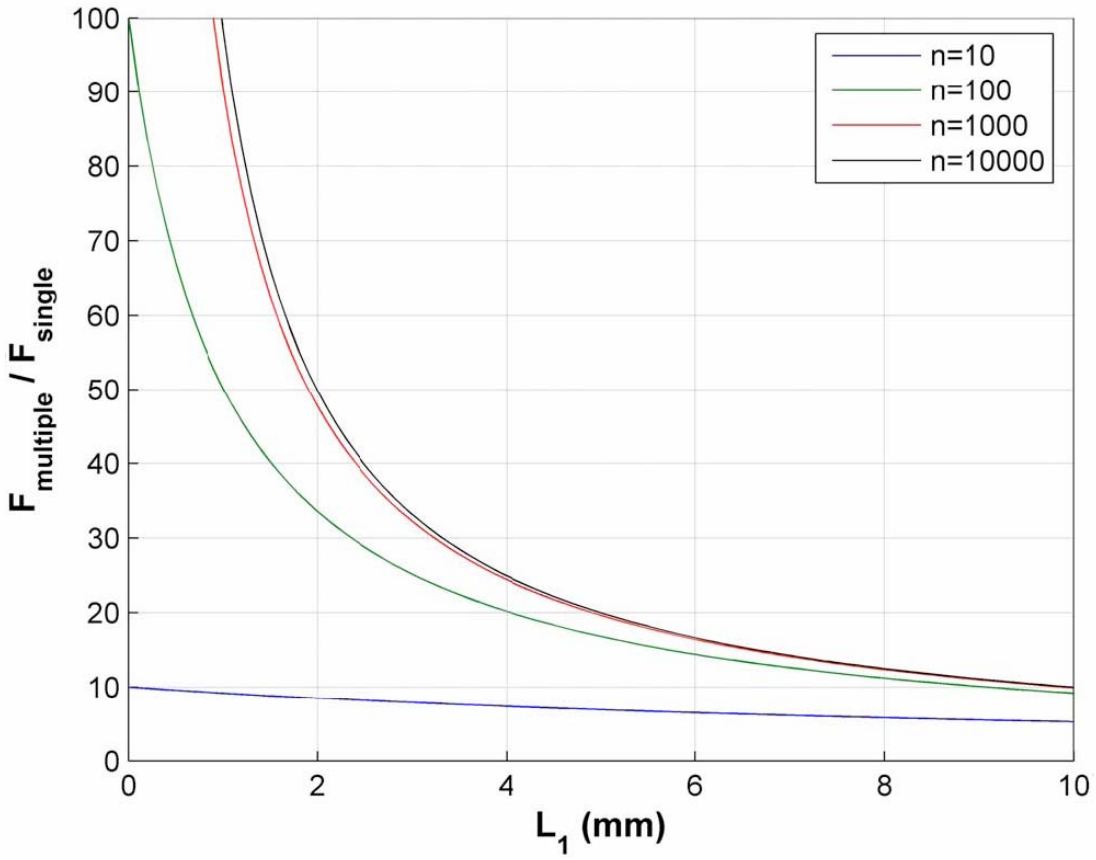

Figure 2.3. Plot of the ratio of fluid flows of multiple channel EOF pump to single channel EOF pump of equal cross-sectional area, as a function of pump segment length L_1. The total length $L_1 + L_2 = 100$ mm, such that as L_1 becomes longer, L_2 becomes shorter. This ratio is shown for several numbers of pump arms.

2.3 Thin Film EOF Pump Fabrication

EOF pumps were fabricated using standard thin film lithography on silicon and glass wafers (Figure 1.1), in an adaptation of earlier work.[19-21] To prevent electrical breakdown when using silicon wafers, a 2.5-μm layer of thermal oxide was grown on each wafer followed by a 200-nm layer of silicon nitride deposited by plasma enhanced chemical vapor deposition (PECVD). This was followed by an additional 300-nm silicon dioxide layer deposited by PECVD. This oxide layer was also applied over the top of the glass to ensure that the pump channel walls consisted of the same material. Next, a 300-nm layer of aluminum was evaporated on the wafer followed by a spin coating of 3-μm AZ3330 photoresist. The photoresist was then patterned and developed. To give the channels a rounded shape, the photoresist was re-flown at 250 ºC. Next, the aluminum was etched in an aluminum etchant (Transene, Danvers, MA), and 3 μm of silicon dioxide were deposited on top of the wafer using PECVD. To open the channels, the channel ends were etched with buffered hydrofluoric acid (Transene) and then submerged in 2:1 HCl/HNO_3 and Nanostrip (Cyantek, Fremont, CA) to remove the sacrificial core consisting of aluminum and photoresist. After core removal, the smaller pump channels were 5 μm wide and 4 mm long, and the larger channel was 50 μm wide and 5 mm long. SEM images of various EOF pump features are shown in Figure 2.4.

2.4 Measurement of Pump Flow Characteristics

A schematic overview of the experimental setup for measuring pump flows is shown in Figure 2.2. Reservoirs to hold solutions over openings at the ends of the microchannels were prepared from laser-cut tube-like pieces of poly(methylmethacrylate) (PMMA) with two 10-cm lengths of 750-μm i.d. Teflon capillary tubing epoxied into the

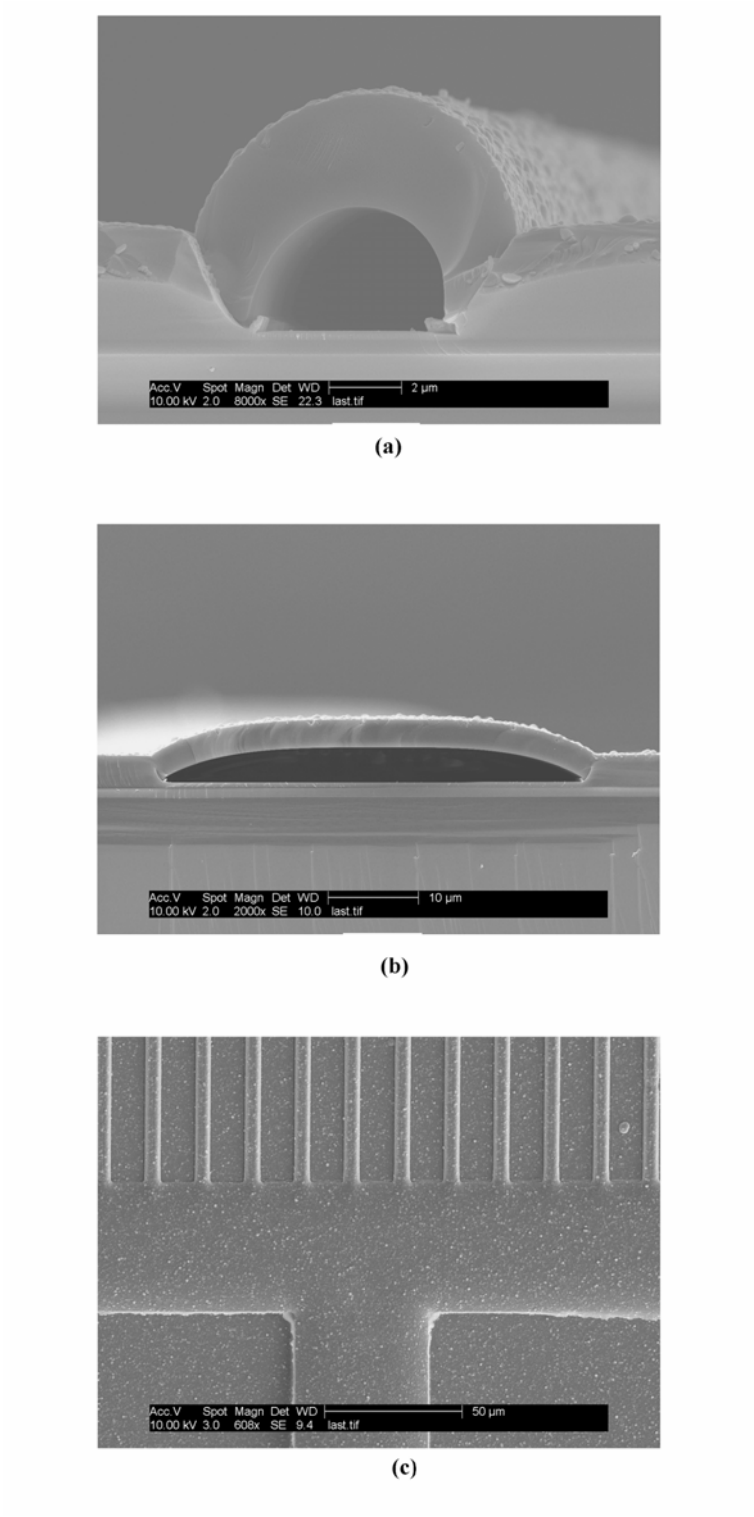

Figure 2.4. SEM images of EOF pump features. (a) Cross-sectional view of a 5-µm EOF channel. (b) Cross-sectional view of a 50-µm flow channel. (c) Top view of the pump channels interfaced with the flow channel.

reservoir. PMMA reservoir material could be easily made into various reservoir sizes using a laser cutter. The large i.d. of the Teflon tubing was selected to make its effect on the overall EOF insignificant. Short lengths of Teflon tubing were used so that buffer solutions could easily be purged from the apparatus, reducing the time between experiments. A carbonate buffer solution (10 mM, pH 9.2) was prepared from sodium bicarbonate and sodium carbonate. To accurately measure flow volumes generated by the EOF pumps, each test was run long enough to easily measure solution displacements in the Teflon tubing. Hydroquinone and *p*-benzoquinone were added to the buffer solution to decrease electrolysis gas generation. Palladium wire was inserted into the top of the capillary tubing to serve as an electrode.[22,23] Palladium was chosen to further decrease the effects of electrolysis by absorbing any hydrogen gas produced.

With each flow-rate experiment, pressurized injections of carbonate solution were made to ensure complete removal of air in the device to prevent blocking of the channel. The current measured when all small channels were working was used for determining whether or not all channels in the other pumps were working.

EOF pumps on both silicon and glass substrates were tested. Graphs of flow rate versus electric field are shown in Figures 2.5 and 2.6. Figure 2.6 shows plots on an expanded scale for the results obtained using single large channels. The flow rate was calculated by measuring the change in volume in the Teflon capillary and dividing by the change in time. As our results indicate, the values for flow rate versus electric field match very closely for the devices built both on silicon and glass substrates. This outcome was expected because the walls of the channels for both substrates were formed from the same type of PECVD-deposited oxide.

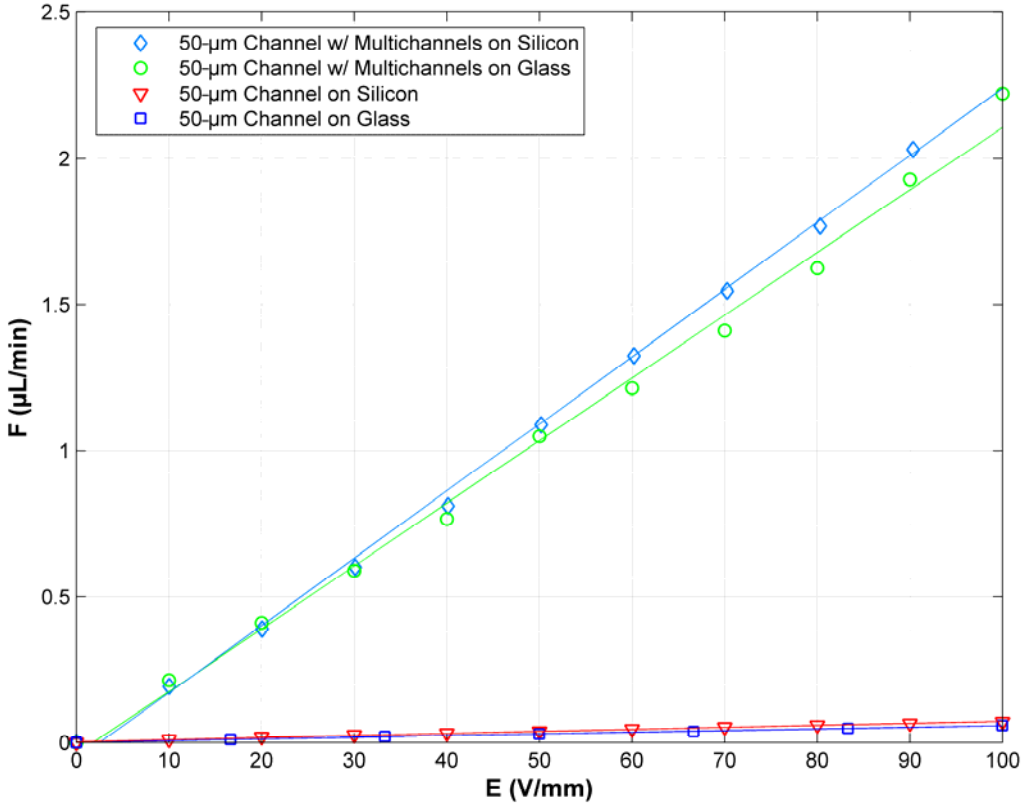

Figure 2.5. Plot of flow rate versus applied electric field for multiple channel EOF pumps and single channel EOF pumps fabricated on silicon and glass substrates.

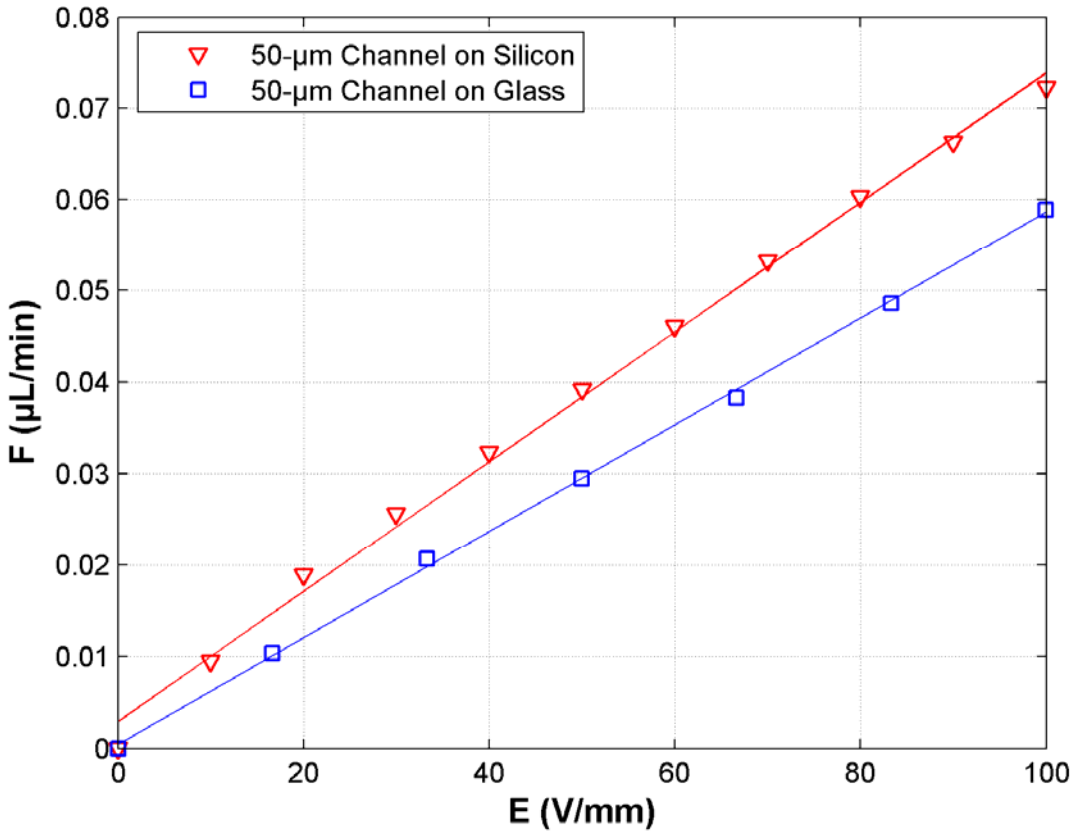

Figure 2.6. Expanded view of the flow rates generated in single 50-µm channel EOF pumps.

2.5 Design Optimization

EOF pump efficiency can be expressed as the ratio of usable mechanical work produced per unit time to the applied electrical power.[24] The flow created in an EOF pump attached to a load results in a backpressure which changes the EOF plug profile to assume a parabolic shape, which is referred to as the pump curve.[25] If it is assumed that the pump curve closely approximates linear behavior over a wide range of applied electric field, the relationship in Equation 2.6 is produced,[25]

$$\frac{\Delta P}{\Delta P_{\max}} + \frac{F}{F_{\max}} = 1 \tag{2.6}$$

The linear relationship shown in Equation 2.6 then leads to the maximum mechanical power that can be produced by the pump,

$$Q_{\max} = \frac{\Delta P_{\max}}{2} \cdot \frac{F_{\max}}{2} = \frac{1}{4} \Delta P_{\max} F_{\max} \tag{2.7}$$

The electrical power being applied to the EOF pump can be expressed as,

$$IV = EL_1I \tag{2.8}$$

where I is the current in the system. It is now possible to express the maximum possible EOF pump efficiency with Equation 2.9,[26]

$$\eta = \frac{\Delta P_{\max} F_{\max}}{4EL_1 I} \tag{2.9}$$

As applications of the EOF pump vary, the corresponding microchannel system can become very complex, leading to difficult theoretical analysis. Fortunately, such a potentially complex arrangement can be combined together into a lumped backpressure

system consisting of a single equivalent channel for efficiency calculation purposes. For the treatment of EOF pump efficiency, the simplest case of a single channel is considered.

In order to more fully expand the efficiency equation represented in Equation 2.9, it is necessary to introduce a relationship for electric power that is dependent on the resistivity of the buffer,

$$EL_1 I = \frac{nA_1 E^2 L_1^2}{L_1 \rho} \tag{2.10}$$

where ρ is the resistivity of the buffer. Now, if Equations 2.3, 2.4, and 2.10 are substituted into Equation 2.9, the following generalized efficiency equation is obtained for an EOF pump system,

$$\eta = \frac{2\pi n \varepsilon_o^2 \varepsilon_r^2 \zeta^2 L_1 L_2 d_1^4 d_2^4 \rho}{\upsilon A_1 (L_1 d_2^4 + n L_2 d_1^4)^2} \tag{2.11}$$

To use this efficiency equation for the thin film fabricated EOF pumps presented in this chapter, the equivalent diameter (d) for the devices must be calculated from the following equation,

$$d = 4A/P \tag{2.12}$$

where A is the cross-sectional area of the microchannel, and P is its perimeter. We can express area by Equation 2.13, and perimeter by Equation 2.14,

$$A = \frac{\pi ab}{2} + 2bm \tag{2.13}$$

$$P = \frac{\pi[3(a+b) - \sqrt{(3a+b)(a+3b)}]}{2} + 2m + 2b \tag{2.14}$$

where a is the height of the channel core, b is the channel half-width, and m is the height of the evaporated aluminum layer. These equations were generated assuming an approximate half-elliptical shape of the core plus the area contributed by the aluminum layer. Due to the fabrication techniques employed, m = 300 nm, a_1 = 2.2 μm, a_2 = 3.5 μm, and b_2 = 25 μm.

Figure 2.7 demonstrates EOF pump efficiencies for 10, 100, and 1000 pump arms over a range of equivalent pump arm diameters. This figure shows that efficiency increases with an increasing number of pump arms and decreasing equivalent pump arm diameter. It can also be inferred from Figure 2.7 that it is possible to select an equivalent diameter to maximize the efficiency of an EOF pump system for a given number of pump arms.

For microfabricated systems, a central aim is to minimize the total device size. Therefore, maximizing the use of the area on the chip is of great importance. EOF pumps can be designed for the most efficient use of space and, therefore, the maximum power for fixed chip area. The maximum mechanical power that an EOF pump system produces can be expressed as the product of the pressure generated in the system (Equation 2.3) times the flow rate (Equation 2.4). This leads to,

$$Q_{mechanical} = \frac{2\pi m \varepsilon_o^2 \varepsilon_r^2 \zeta^2 d_1^4 d_2^4 L_2 V^2}{\upsilon L_1 (L_1 d_2^4 + n L_2 d_1^4)^2} \tag{2.15}$$

where V is the voltage drop across the pump. As an example of the use of Equation 2.15, three different EOF pump shapes that occupy an equal chip area were compared. Assuming that all three designs have the same spacing between pump arms and the same pump arm diameter, the on-chip area is $2nwL_1$, where w is the width of one pump arm.

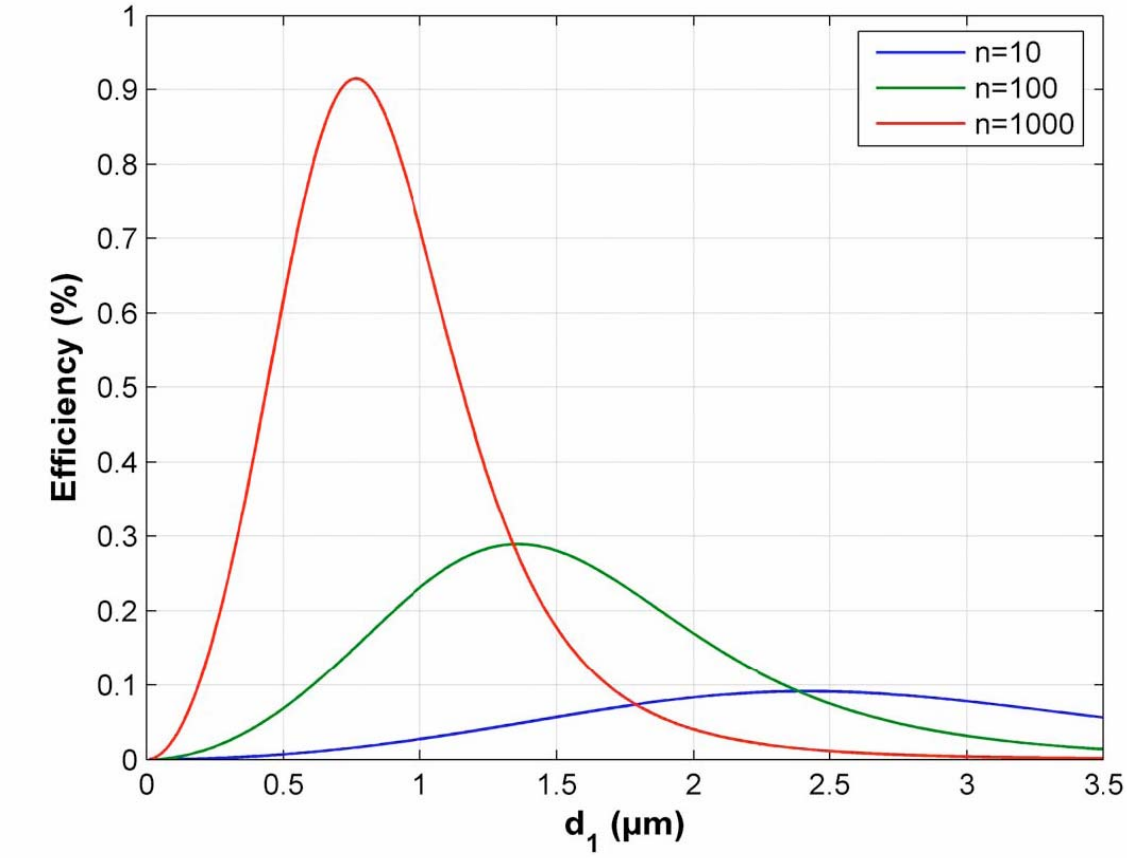

Figure 2.7. Plot of efficiency of an EOF pump system having EOF pump channels that are 4 mm long. The pump channels are attached to a 5-mm long, 50-μm wide single channel.

For a square design, the total width and length of the pump are equal, leading to $L_1 = 2nw$. A rectangular shape that is four times as long as it is wide leads to $L_1 = 8nw$. A rectangle, which is four times as wide as it is long, leads to $L_1 = 1/2nw$. Given an on-chip area of 1 cm², and typical values for channel lengths and diameters (L_2 = 5 mm, w_1 = 5 μm, w_2 = 50 μm, a_1 = 2.2 μm, and a_2 = 3.5 μm), Equation 2.15 leads to the results shown in Figure 2.8. The greatest mechanical power is generated by the short EOF pump with many pump arms at $(4.1 \times 10^{-15})V^2$ W, while the least efficient is the long EOF pump with fewer pump arms at $(3.4 \times 10^{-15})V^2$ W. If possible, using a short, wide design would be preferable from a chip area efficiency standpoint.

2.6 Conclusions

Due to the multiple-channel structure of the EOF pump, much higher pressures and flow rates can be achieved compared to a single microchannel of equal cross-sectional area. The measured flow rates agree well with EOF pump theory, and also demonstrate the reproducibility of EOF pump performance. Highest pump efficiency is achieved using very small-diameter pump arms. For a given total chip area, EOF pump power is maximized using many short pump arms rather than fewer long pump arms. The implementation of EOF pumps in microfluidic systems can be greatly facilitated through the ease and precision of thin film fabrication techniques, as well as through on-chip integration. For example, EOF pumps can be integrated on-chip with other microfluidic systems as the driving force for liquid chromatography with monolith and gel packed channels, or as a microelectronic cooling pump.

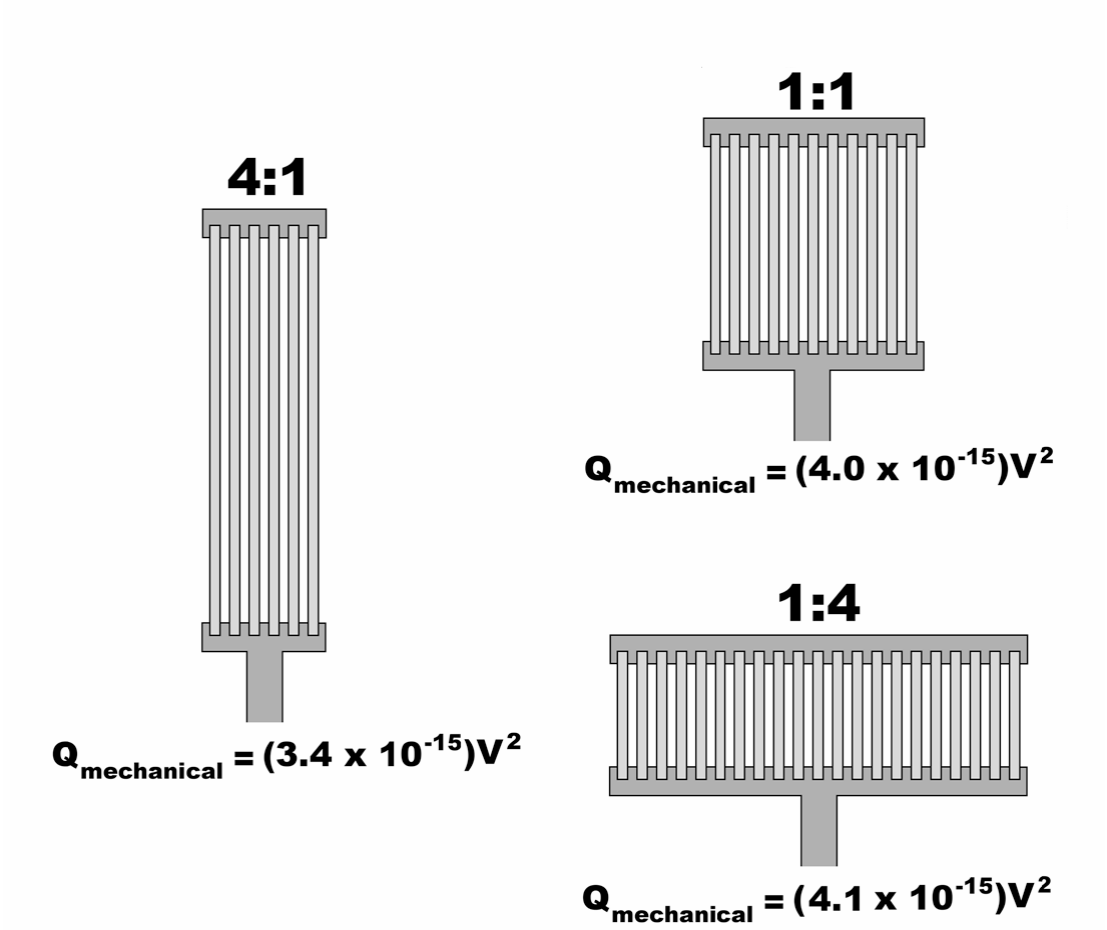

Figure 2.8. Schematic of three different pump configurations of equal cross-sectional area. The configurations differ by length-to-width ratios of 1:1, 4:1, and 1:4. Mechanical power ($P_{mechanical}$) increases with pump width. For these calculations, the pump arms were 2.5 µm tall and 5 µm wide.

2.7 References

1. Laser, D. J.; Santiago, J. G. *J. Micromech. Microeng*. **2004**, *14* R35–R64.
2. Ajdari, A. *Phys. Rev. E*, **1996**, *53*, 4996-5005.
3. Hiemenz, P. C.; Rajagopalan, R. Eds. Principles of Colloid and Surface Chemistry, Third Edition, Revised and Expanded, Marcel Dekker, New York, 1997.
4. Santiago, J. G. *Anal. Chem*. **2001**, *73*, 2353-2365.
5. Pretorius, V.; Hopkins, B. J.; Schieke, J. D. *J. Chromatogr*. **1974**, *99*, 23-30.
6. Raymond, D. E.; Manz, A.; Widmer, H. M. *Anal. Chem*. **1994**, *66*, 2858-2865.
7. Ramsey, R. S.; Ramsey, J. M. *Anal. Chem*. **1997**, *69*, 1174-1178.
8. Liu, S.; Pu, Q.; Lu, J. J. *J. Chromatogr. A* **2003**, *1013*, 57-64.
9. Nischang, I.; Chen, G.; Tallarek, U. *J. Chromatogr. A* **2006**, *1109*, 32-50.
10. Pu, Q.; Liu, S. *Anal. Chim. Acta*. **2004**, *511*, 105-112.
11. Lazar, I. M.; Karger, B. L. *Anal. Chem*. **2002**, *74*, 6259-6268.
12. Liu, S.; Dasgupta, P. K. *Anal. Chim. Acta*. **1992**, *268*, 1-6.
13. Dasgupta, P. K.; Liu, S. *Anal. Chem*. **1994**, *66*, 1792-1798.
14. Chen, L.; Ma, J.; Guan, Y. *J. Chromatogr. A* **2004**, *1028*, 219-226.
15. Tripp, J. A.; Svec, F.; Frechet, J. M. J.; Zeng, S.; Mikkelsen, J. C.; Santiago, J. G. *Sens. Actuators B* **2004**, *99*, 66-73.
16. S. Zeng, S.; Chen, C.; Mikkelsen Jr., J. C.; Santiago, J. G. *Sens. Actuators B* **2001**, *79*, 107.
17. Paul, P. H.; Garguilo, M. G.; Rakestraw, D. J. *Anal. Chem*. **1998**, *70*, 2459-2467.
18. Rice, C. L.; Whitehead, R. J. *Phys. Chem*. **1965**, *69*, 4017-4024.

19. Barber, J. P.; Conkey, D. B.; Lee, J. R.; Hubbard, N. B.; Howell, L. L.; Schmidt, L.; Hawkins, A. R. *IEEE Photon. Technol. Lett*. **2005**, *17*, 363.

20. Barber, J. P.; Lunt, E. J.; George, Z. A.; Yin, D.; Schmidt, H.; Hawkins, A. R. IEEE Photon. Technol. Lett. **18**, 28 (2006).

21. Peeni, B. A.; Conkey, D. B.; Barber, J. P.; Kelly, R. T.; Lee, M. L.; Woolley, A. T.; Hawkins, A. R. *Lab Chip* **2005**, *5*, 501-505.

22. Chen, D. C.; Hsu, F. L.; Zhan, D. Z.; Chen, C. H. *Anal. Chem*. **2001**, *73*, 758-762.

23. McKnight, T. E.; Culbertson, C. T.; Jacobson, S. C.; Ramsey, J. M. *Anal. Chem*. **2001**, *73*, 4045-4049.

24. Griffiths, S. K.; Nilson, R. H. *Electrophoresis* **2005**, *26*, 351-361.

25. Wang, P.; Chen, Z.; Chang, H. C. *Sens. Actuators B* **2006**, *113*, 500-509.

26. Chen, C. H.; Santiago, J. G. *J. Microelectromech. Syst*. **2002**, *11*, 672-683.

3 CHARACTERIZATION OF THIN FILM MICROFLUIDIC DEVICES

3.1 Background

To correctly predict the electroosmotic flow rate in a microfluidic channel, it is necessary to first understand the properties of the surface. Silicon dioxide surfaces readily hydrolyze to form silanol groups. These surfaces are easily charged by becoming protonated or deprotonated when in the presence of an acidic or basic solution. A charged surface in the presence of an ionic solution and an electric field generates electroosmotic flow. As mentioned earlier, the flow rate is directly proportional to the zeta potential, which in turn is a function of the surface properties. Physical irregularities in the surface affect the zeta potential and must be eliminated (or accounted for) to correctly predict the flow rate.[1,2] PECVD silicon dioxide is amorphous, unlike thermally produced silicon dioxide which is crystalline.[3,4] PECVD oxide is also polymeric in nature, forming occasional covalent bonds with neighboring layers.[3,4] This results in a silicon dioxide structure which is less dense than thermal silicon dioxide. The physical and electrical properties of thermal silicon dioxide are well known, but may be somewhat different for PECVD silicon dioxide.[3,4] PECVD silicon dioxide can be changed by altering the growth parameters, and are specific to each PECVD system.[3,4] Therefore, accurate knowledge of the surface structures of silicon dioxide devices is essential. In this chapter, I have investigated the electrical properties of PECVD silicon dioxide as well as methods to predict and control devices fabricated with PECVD silicon dioxide to improve the quality of the devices and their performance.

3.2 Zeta Potential Determination

To better understand the channel surface of the multichannel EOF pump used in Chapter 2, the zeta potential was calculated at several different pH levels.[5] Using the same set-up and method described in Chapter 2 to measure the EOF, the zeta potential of the silicon dioxide was measured. The pH ranged from 2.6 to 8.3 for multiple electric field strengths.[5] The buffer concentration of each pH solution was 10 mM with ionic strengths ranging from 4 to 30 mM.[5] Figure 3.1 is a graph showing the calculated zeta potential versus pH. The zeta potential was found by rearranging the cylindrical capillary model for electroosmotic flow reported by Rice and Whitehead,[7]

$$Q_{EOF} = \frac{\pi \varepsilon_o \xi E d^2}{4\eta} \tag{3.1}$$

From Figure 3.1 the zeta potential of the PECVD oxide surface can be interpolated for a specific pH. Now that the zeta potential is known the EOF can be calculated for different channel diameters and pH values.

3.3 Quality Control

Unexpected changes in the EOF can result from different conditions, such as contaminants, device cracks, etc. (Figure 3.2). During the process of determining the zeta potential and EOF rates in Section 3.2 and in Chapter 2, several problems were encountered that led to a systematic check-list on how to quickly tell if a device is functional and, in some cases, how to restore the surface quality. From working with hundreds of devices, I have devised a simple set of steps to determine device quality. These areas can be divided into initial testing and post reservoir application filling.

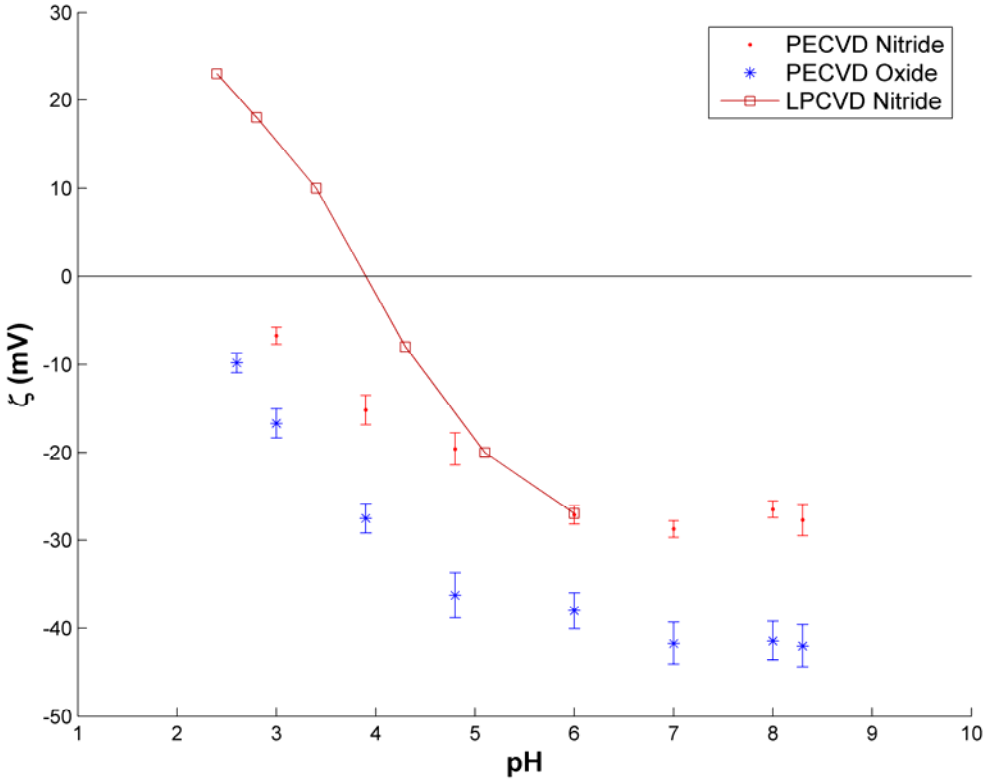

Figure 3.1. Experimental zeta potential (ζ) versus pH for PECVD silicon oxide and nitride.[5,6]

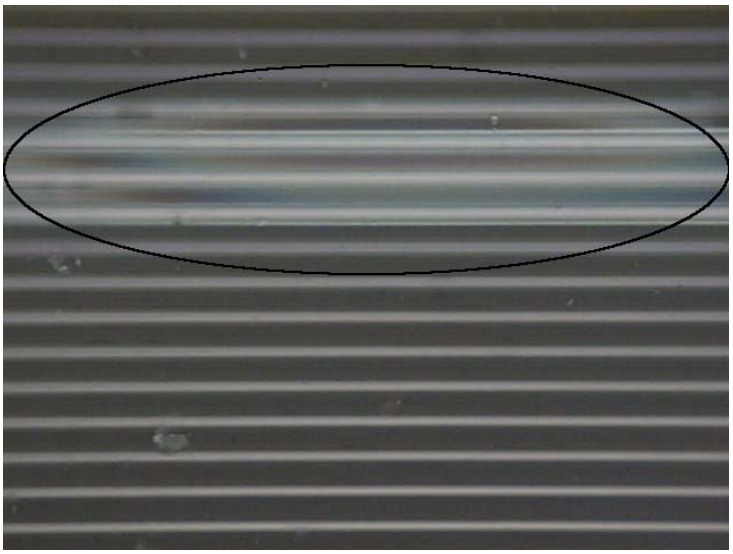

(a)

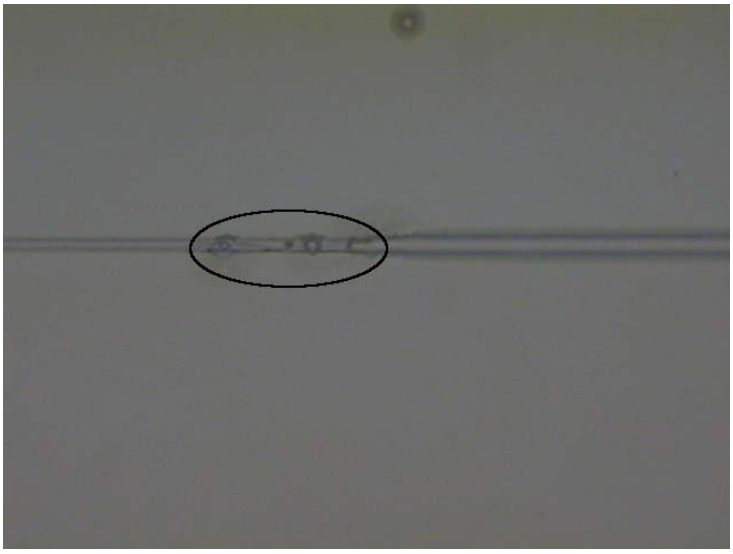

(b)

Figure 3.2 Photographs of (a) contaminants and (b) cracks in channels, which are detrimental to the zeta potential and EOF rate in a device.

3.3.1 Initial Testing

Initial testing can be used to identify over 90% of the defective microchannels. The first step is to orient the wafer with respect to a light source to observe the reflection. If the wafer appears to have a rainbow-like film on it, then it is dirty and must go through the cleaning cycle again (overnight in Nanostrip and then 4 h in acetic acid). Once the wafer is clean, then the wafer must be visually inspected under the microscope. Any defects such as broken channels, cracks, etc., on a wafer indicate structural problems in the device. An additional step is to place a drop of water on the channel opening to fill the channels by capillary action to observe if they fill completely. After the integrity of a channel configuration has been verified, then reservoirs may be glued on the appropriate positions.

3.3.2 Post Reservoir Attachment Testing

Sometimes after reservoirs have been attached, the channels will no longer fill. This problem is worse for pump segments because they contain multiple channels. The first step in evaluating devices after reservoir attachment is to check for air bubbles. Sometimes bubbles get caught in the channel as fluid moves through the channel (Figure 3.3). The bubbles seem to stop where there are rough spots on the surface. The easiest way to remove a bubble is to apply vacuum to the open end of the channel. If this does not work, the solution should be removed, and the channel refilled. Sometimes channels do not fill because a bubble gets caught at the bottom of the reservoir; such bubbles are easily removed by mixing the solution with a syringe needle. The second most common problem is that the epoxies used to attach the reservoirs enter and clog the channel. This

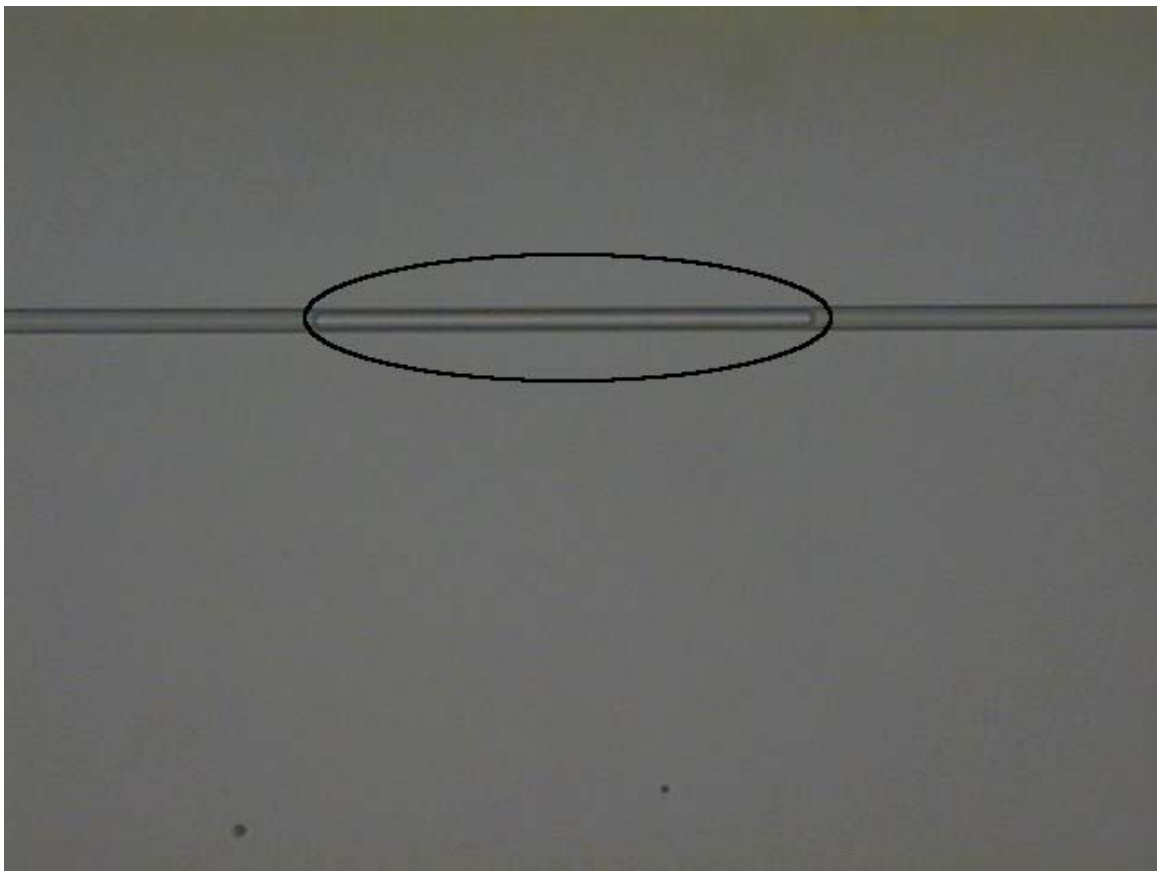

Figure 3.3 Photograph of a bubble that is trapped in a channel.

happens at the channel opening and, also, if there are small cracks in the channel. Both cases can usually be seen under the microscope. If the channel is cracked, nothing can be done to resolve the problem; however if the openings were accidentally filled with epoxy, then the epoxy can be removed by placing the device in Nanostrip overnight and then in acetic acid for about 4 h.

3.4 References

1. Dutta, P.; Beskok, A. *Anal. Chem*. **2001**, *73*, 1979-1986.
2. Grimes, B. A.; Liapis, A. I. *J. Colloid Interface Sci*. **2003**, *263*, 113-118.
3. Konuma, M. Plasma Techniques For Film Deposition. (Alpha Science, Harrow, UK, 2005).
4. Sivaram, S. Chemical Vapor Deposition: Thermal and Plasma Deposition of Electronic Materials. (Van Nostrand Reinhold, New York, 1995).
5. Hamblin, M. N.; Edwards, J. M.; Lee, M. L.; Woolley, A. T.; Hawkins, A. R. *Biomicrofluidics*, **2007**, *1*, 034101-034106.
6. Bousse, L.; Mostarshed, S. *J. Electroanal. Chem. Interfacial Electrochem*. **1991** *302*, 269.
7. Rice, C. L.; Whitehead, R. J. *Phys. Chem*. **1965**, *69*, 4017-4024.

4 SELECTIVE SURFACE MODIFICATION OF CHANNELS IN THIN FILM MICROFLUIDIC DEVICES

4.1 Surface Modification Procedure and Testing

With the successful integration of EOF pumps into microfluidic devices, the next goal was to show that the pump could be used to separate a mixture based on capillary liquid chromatography. The target analytes were amino acids and several neutral fluorescent molecules. Separation of these analytes would demonstrate that the pump could generate enough pressure to produce hydrodynamic flow through the separation channel for microfluidic separations.

The goal was to coat the surface of the separation channel with a silanizing agent, chlorooctadecyldimethylsilane (Sigma Aldrich, St. Louis, MO), following a procedure adapted from Kutter *et al.*[1,2] Glass reservoirs were attached to the channel openings. A solution containing a silanizing agent was prepared in toluene which had been dried with a sieving alumina matrix. The silanizing agent was added to toluene (Sigma Aldrich, St. Louis, MO) so that it was approximately 10% (w/w). Next, 1-2 μL of n-butylamine (Sigma Aldrich) was added to the solution as the catalyst. The solution was added to the reservoir and filled the channels by capillary action. The solution was left in the channel for approximately 15 min and then vacuum was applied at the outlet end to remove the solution, and the channels were refilled. This procedure required approximately 1 h to perform. Afterwards, excess silanizing agent was removed from the channels by rinsing with toluene and then methanol. Analyte solutions were prepared by combining 600 μL each of 3 mM solutions of arginine, glycine, and phenylalanine (ICN Biomedicals, Aurora, OH) with 200 μL of 6-mM fluorescein 5-

isothiocyanate (FITC; Molecular Probes, Eugene, OR). To complete the labeling process, the solution was placed in the dark at room temperature for 4 days. Next, sample solutions were prepared by combining the amino acids and diluting the concentration to 5 μM in 10 mM Tris buffer, pH 8.2. Finally, a 10-μL volume of the solution was pipetted into the reservoir for separation.

The primary microfluidic device design in this work included two pumps as can be seen in Figure 4.1(a). This design was chosen because both sample injection and separation could be operated independently by applying voltage to one pump or the other. The sample reservoir was chosen as one of the pumps. The analytes were detected by a LIF detection system as described by Fuentes *et al*.[2] and Kelly *et al*.[3] The Ar ion laser wavelength was 488 nm. The beam was directed to an inverted microscope where a photomultiplier tube (PMT) collected the signal using a LabView (National Instruments, Austin, Texas) program that was programmed to sample at 100 Hz.

During this work, many problems were encountered. The most difficult problem was interfacing external equipment such as vacuum and pumps with the device. I first used vacuum and pressure to try to control the penetration of coating solution in the channel in order to select the regions to be functionalized. If the reagent entered the pump channels, the EOF would be compromised. After many attempts, I was unable to control the fluid flow. The capillary action increased greatly with the increased surface area of the pumps so that the pumps rapidly filled with silanizing agent. An idea that was tried to solve this problem was to fill the pumps first with toluene and then apply vacuum to draw the silanizing solution out through the other channel. This was also

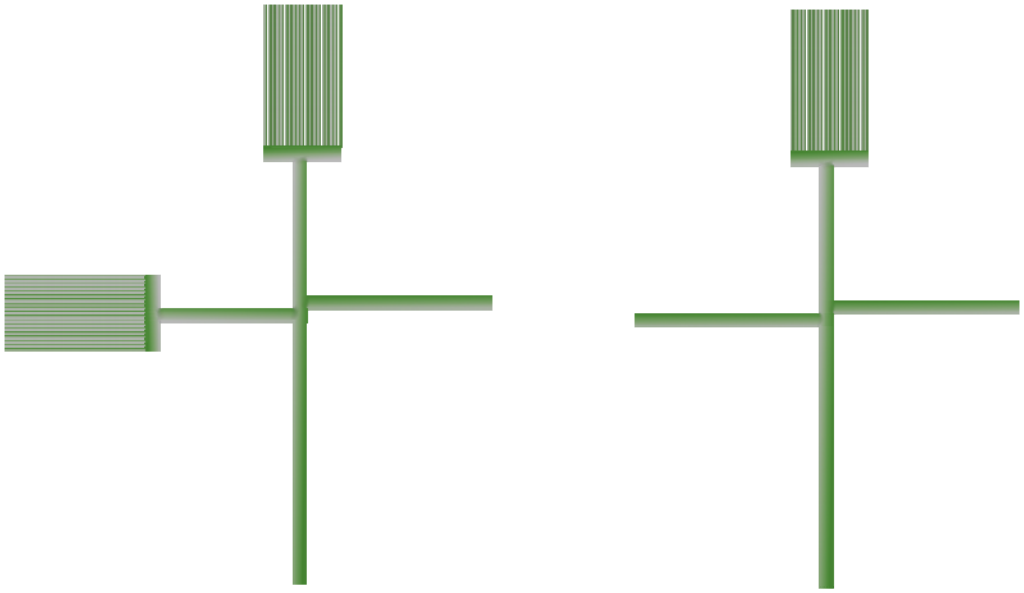

(a) **(b)**

Figure 4.1 Microfluidic channel designs for surface modification experiments using (a) two EOF pumps and (b) a single EOF pump.

unsuccessful because the vacuum was more effective in drawing the toluene solution, and the silanizing agent only entered part of the device channel. Other attempts to functionalize the channel included blocking the channel with photoresist and PEG. PEG was soluble in toluene and, therefore, the complete pump was functionalized. Photoresist did seem to stop the solution from entering the pump, but other problems were expected such as fouling of the surface and side reactions with the silanizing agent. AZ3330 and AZ3312 were both used to block channels (Figure 4.2). It seemed that a mixture of the two was the best to control how far the photoresist entered the pump. In addition to the mixture ratio of the photoresists, the drop size placed on the channel was crucial. The larger the drop size, the farther the photoresist entered the channel. Photoresist in the channels could be easily removed with acetone.

Another problem encountered was the use of epoxy to cement the reservoirs. In the past, various epoxies such as 5-Minute epoxy (ITW Devcon, Danvers, MA) and Loctite, Hysol 1C (Henkel, Hayward, CA) were exclusively used. Toluene dissolves 5-Minute epoxy and therefore was not used to glue on the reservoirs. Loctite epoxy worked well with toluene solutions, however, later on when the devices were tested, it was found that this epoxy was slowly dissolved in water. Also, as a side note, it was found that the 5-Minute epoxy was soluble in water but at a much slower rate. To solve these problems, numerous epoxies were researched and tested. The best solution to this problem was 3M 2216 B/A (St. Paul, MN). This is a rubber-like epoxy that is highly viscous and adheres very well. After multiple tests, the 2216 epoxy was proven resistant to both toluene and water for several days. It also adhered better than the other

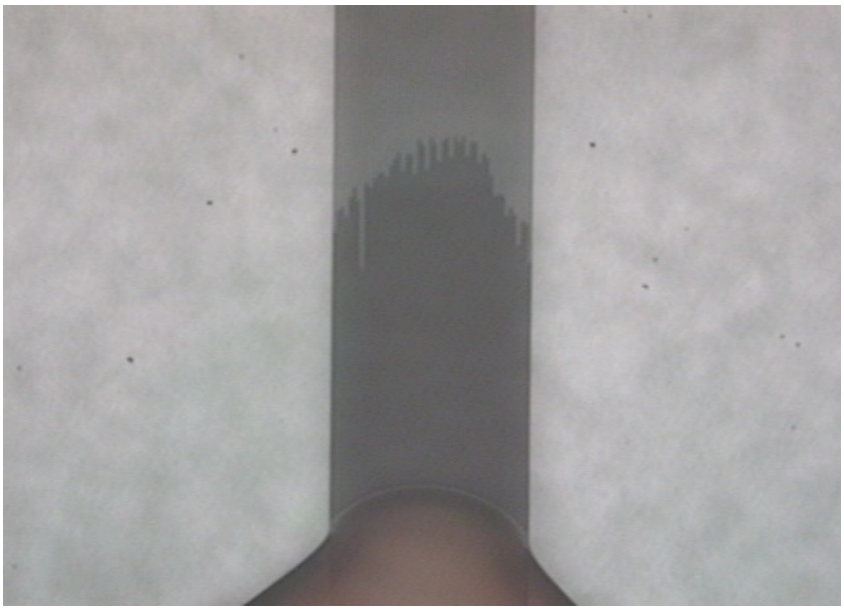

(a)

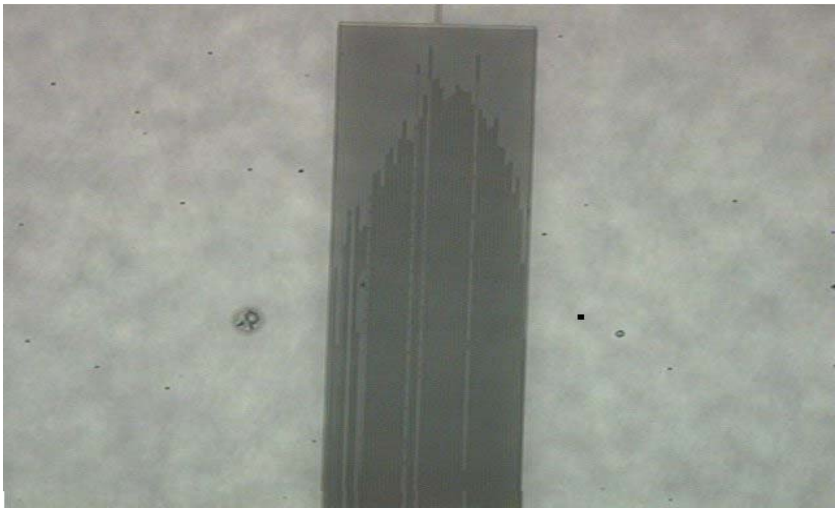

(b)

Figure 4.2 Photographs of channels being filled with (a) photoresist AZ3330 and (b) photoresist AZ3312.

epoxies, which meant that less epoxy was needed to attach the reservoirs. The main disadvantage to using this epoxy was that it took longer to cure (almost 24 h).

The third problem encountered was complete filling of the device with buffer and water solutions. It was important to consistently and completely fill the channels to keep the electrical current and flow rate consistent. Current and flow rate fluctuations cause changes in the separation time, thereby reducing the separation reproducibility. Small air bubbles in a channel can also distort the chromatographic peaks. The bubble removal method described in Chapter 3 helped, but did not eliminate all problems involving air bubbles; therefore, I tried filling the device from both the pump end and the large channel end in combination with the bubble removal technique. As Figure 4.3 shows, the devices do not fill completely when they were filled from the larger channel. Channels fill best when they fill from the pump; however, a small bubble often became stuck in the larger channel. After careful monitoring, I found that this bubble originated from larger bubbles that were being pushed out by capillary action in the pump. As a large bubble traveled down the channel, a small bubble broke off from the main bubble and stayed in the channel. This was probably due to irregularities on the channel surface. This was common in the majority of devices, but occasionally the bubble could not be removed. Another more successful approach to fill the devices was to use recently commercialized Microports (Cascade Microtech, Beaverton, OR). Microports are manufactured reservoirs made of polyetheretherketone (PEEK) that have a silicone tip which can be conveniently pressed against the channel opening. A syringe pump can then be connected to the microport system to introduce fluid into the channel. The microport system removed all of the air bubbles, but could not be used as a permanent

reservoir because of the presence of toluene in the silanizing solution which could dissolve the silicone.

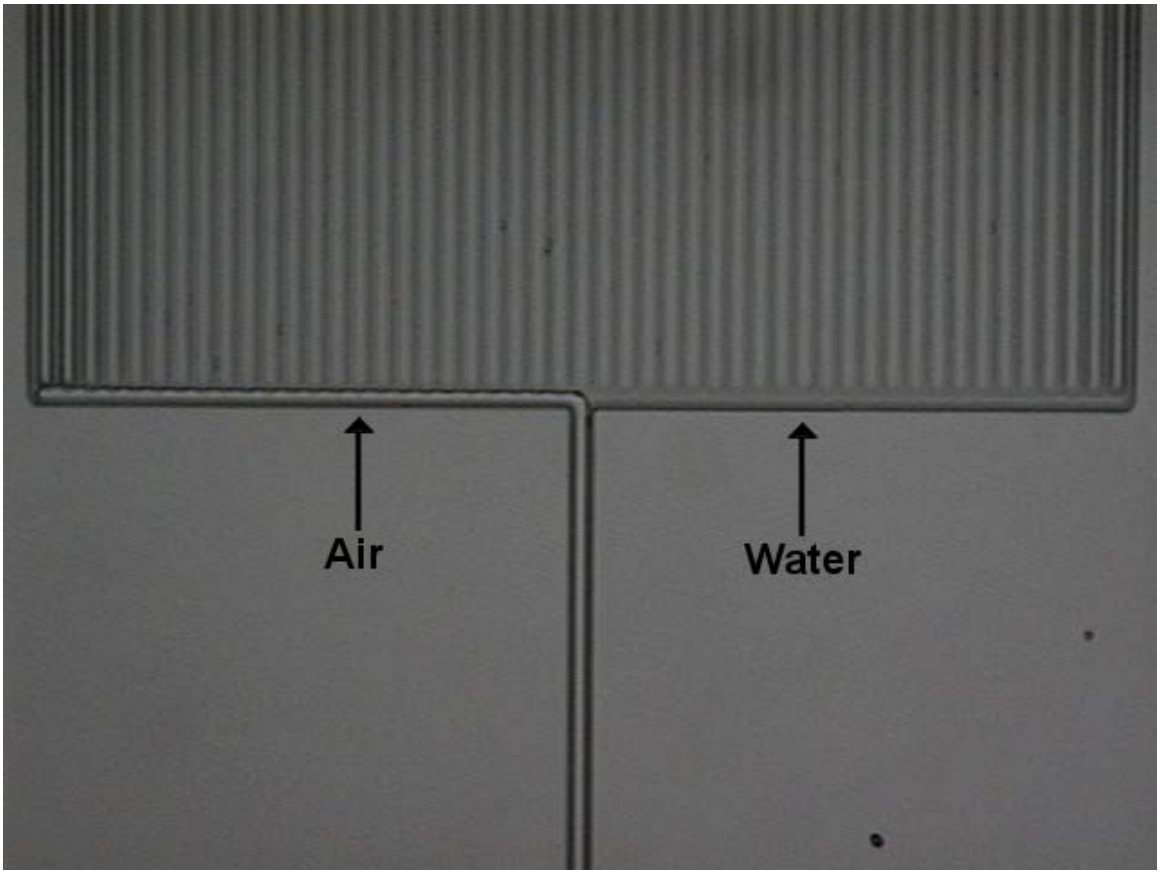

Figure 4.3 Photograph of filling pattern of an electroosmotic pump in which the filling originated with the large channel.

4.2 References

1. Kutter, J. P.; Jacobsen, S. C.; Matsubara, N.; Ramsey, J. M. *Anal. Chem*. **1998**, *70*, 3291-3297.

2. Fuentes, H. V.; Woolley, A. T. *Lab Chip* **2007**, **DOI:** 10.1039/b708865e.

3. Kelly, R. T.; Woolley, A. T. *Anal. Chem*. **2003**, *75*, 1941-1945.

5. CONCLUSIONS AND FUTURE WORK

5.1 Conclusions

The research presented here shows the progress that has been made in creating a miniaturized EOF pump. The initial research by Barber and Peeni *et al*.[1,2] led to the current thin film fabrication techniques, and they demonstrated that such devices could be used to separate amino acids. As demonstrated in this work, it is possible to integrate a pump onto a microchannel that is capable of generating reasonable pressures. It was found to be difficult in this work to coat a stationary phase in the separation channel of a microfluidic system that contained integrated EOF pumps. This must be eventually resolved before microfluidic LC separations can be demonstrated. The next step is to show that a EOF pumps can be used to separate a mixture of charged and neutral molecules.

5.2 Future Work

5.2.1 Coating the Integrated Separation Channel

A single pump configuration, such as shown in Figure 4.1(b) would be easier to control fluid penetration. However, it would be best to coat the larger channel surface after blocking the pumps with photoresist. Then the same surface treatments as mentioned in Chapter 4 could be done. After functionalizing the channel, the photoresist could be removed with acetone and the channel filled with buffer. With a coating on the surface, bubble adhesion in the main channel should be eliminated as the pump is filled with the analyte solution. The rest of the process should be straightforward.

5.2.2 Optical Wave Guides for On-Chip Detection

Silicon substrates are not easily used in CE separations because they lack optical transparency for LIF detection. A new method using thin film fabrication[1,2] methods can be used to create anti-resonant reflective optical waveguides (ARROWs). These waveguides consist of multiple layers of silicon dioxide and silicon nitride.[1] The advantage of using ARROWs for silicon devices is that they allow for horizontal detection, because the thin film layers are optically transparent, whereas the silicon substrate is opaque.[3] The waveguides are connected to conventional waveguides, which in turn are connected to a laser and detector. ARROWs allow the possibility of total integration of a detector on the microchip. In the future, there is the possibility that LEDs and even the detector can be fabricated on the surface, removing the need for external lasers and detectors. Recently Hamblin *et al.*[4] classified the surfaces of both PECVD silicon dioxide and nitride films. It was shown that the surface of silicon nitride PECVD films are primarily silanol groups,[4] which generate electroosmotic flow in the microfluidic channel. In the future, it will be possible to include an electroosmotic pump with an ARROW-containing microfluidic device.

5.2.3 Conductivity Detection

Conductivity or electrochemical detection is currently being explored to detect analytes in CE. The idea of using conductivity detection was developed first for CITP in the 1970s.[5] Recently, there has been a renewed interest in conductivity detection because it can be simply constructed and miniaturized. Unlike LIF, the analytes do not need to be tagged with fluorophore or chromophore molecules. This alleviates one

preparation step and also removes the unreacted chromophore or fluorophore peak that often appears. There is however a potential problem that the applied separation voltage may interfere with the detection signal. Conductivity detection is a universal detection technique; the impedance change is measured as molecules pass by the electrode.[6-10] Contact pads can be placed either in direct contact or not with the solution. Along with analyte oxidation at the anode and reduction at the cathode, electrolysis also occurs, which requires low electric field strengths.[8] In many cases, conductivity detectors have good sensitivity and have been shown to have detection limits as low as 8.0 nM.[10]

With new advances in detection set-ups using conductivity and LIF detection, the goal to create a μTAS will eventually be realized. The EOF pumps used in Chapters 2 and 3 have shown that adequate flow rates can be generated in a microfluidic device, which can be integrated in the future with a detector and separation method. These lab-on-a- chip devices should prove useful because of their compact size, high throughput, selectivity, and speed.

5.3 References

1. Barber, J. P.; Conkey, D. B.; Lee, J. R.; Hubbard, N. B.; Howell, L. L.; Schimdt, H.; Hawkins, A. R. *IEEE Photonics Tech. Lett.* **2005**, *17*, 363-365.
2. Peeni, B. A.; Conkey, D. B.; Barber, J. P.; Kelly, R.; Lee, M. L.; Woolley, A. T.; Hawkins, A. R. *Lab Chip* **2005**, *5*, 501-505.
3. Brown, M.; Vestad, T.; Oakey, J.; Marr, D. W. M. *Appl. Phys. Lett*. **2006**, *88*, 134109-1-134109-3.
4. Hamblin, M. N.; Edwards, J. M.; Lee, M. L.; Woolley, A. T.; Hawkins, A. R. *Biomicrofluidics* **2007**, 034101-034106.
5. Verheggen, T. P. E. M.; van Ballegooijen, E. C.; Massen, C. H.; Everaerts, F. M. *J. Chromatogr*. **1972**, *64*, 185-189.
6. Solinova, V; Kasicka, V. *J. Sep. Sci.* **2006**, *29*, 1743-1762.
7. Grab, B.; Siepe, D.; Neyer, A.; Hergenroder, R. *J. Anal. Chem.* **2001**, *371*, 228-233.
8. Guijt, R. M.; Baltussen, E.; van der Steen, G.; Schaasfoort, R. B. M.; Schaultmann, S.; Billiet, H. A. H.; Frank, J.; van Dedem, G. W. K.; van den Berg, A. *Electrophoresis* **2001**, *22*, 2537-2541.
9. Kuban, P.; Sterbova, D.; Kuban, V. *Electrophoresis* **2006**, *27*, 1368-1375.
10. Galloway, M; Stryjewski, W.; Henry, A.; Ford, S. M.; Llopis, S.; McCarley, R. L.; Soper, S. A. *Anal. Chem*. **2002**, *74*, 2407-2415.